Stratospheric Analysis and Forecasting in the Northern Winter of 1999/2000: The NASA DAO's GEOS-3 System

Steven Pawson

Data Assimilation Office, NASA GSFC, Greenbelt, MD, USA
and
Goddard Earth Sciences and Technology Center, UMBC, MD, USA

David Lamich, Andrea Ledvina, Robert Lucchesi, Tommy Owens
General Sciences Corporation, Beltsville, MD, USA
and
Data Assimilation Office, NASA GSFC, Greenbelt, MD, USA

Paul A. Newman
Atmospheric Chemistry and Dynamics Group, NASA GSFC, Greenbelt, MD, USA

For submission to J. Geophys. Res. – Atmospheres

Version 3.1: June 19, 2002

Abstract

An evaluation is presented of the performance in the northern winter 1999/2000 of the GEOS-3 troposphere-stratosphere data assimilation system (DAS). The impacts of the two main input data types are assessed: upper-air soundings (sondes) provide wind and temperature information and satellite-based (Tiros Operational Vertical Sounders: TOVS) give estimates of the thermal structure. It is shown that in the low stratosphere (300-70hPa) the analyses are generally slightly warmer than the sonde data, but colder than the TOVS data; this relationship reverses between 70 and 10 hPa. There are geographical biases, related to the spatial and temporal coverage of the observation types and to the statistical weights assigned to them in the DAS. Forecasts show a tendency to reduce zonal asymmetries in the atmospheric flow and to suppress stratospheric temperature minima. In the DAS, the analysis increments compensate for this, but it leads to important biases in the multi-day forecasts. The analysis increments are as large as the diabatic forcing in the lower polar stratosphere, indicating a substantial model bias. The results provide important insights into the roles of different data types and the circulation model in producing accurate analyses for studies of polar chemistry and physical processes.

1. Introduction

NASA's Data Assimilation Office (DAO) has developed and maintains an operational capacity for producing real-time analyses and forecasts of the atmosphere. This is known as the Goddard Earth Observing System (GEOS) Data Assimilation System (DAS). Previous versions of the DAS were described by *Schubert et al.* [1993], who focused on the tropospheric system (GEOS-1), and *DAO* [1996], which provided comprehensive documentation of the GEOS-2 troposphere-stratosphere system. Section 2 of this paper will provide a brief description of some relevant aspects of the GEOS-3 system, which has been operating since November 1999, in support of the EOS-Terra satellite. The operational products of the GEOS-3 DAS are six-hourly analyses along with twice daily five-day forecasts (for 0000 and 1200UT). These products contain meaningful information between the surface and the stratopause.

There are two main foci of this study: to validate the analyses, examining data and model impacts, and to assess the quality of the forecasts, emphasizing the high-latitude lower and middle stratosphere during the northern winter of 1999/2000. This was a time of intense observation during the Solve-Theseo (SAGE-3 Ozone Loss and Validation Experiment -- Third European Stratospheric Ozone Experiment) campaign. This study was motivated by the DAO's participation in the field, providing meteorological analyses and forecasts for flight planning and data analysis. The campaign, which included aircraft and balloon measurements, was based mainly in Kiruna, Sweden. Solve-Theseo focused on polar ozone, particularly on dynamical and chemical contributions to ozone depletion in the polar lower stratosphere [*Newman et al.*, 2002]. The quality of meteorological analyses in this region is this of paramount importance to the mission. The most critical aspect of the analyses is the accuracy of the temperature fields, since they affect the formation of polar stratospheric clouds

(PSCs); diagnosis and prediction of PSC formation and evolution depends critically on the adequacy of the temperature analyses.

The first objective, to validate the analyses, complements a number of previous studies that have compared meteorological analyses against either *in-situ* data or against other analyses. *Knudsen* [1996] examined analyses from the European Centre for Medium-Range Weather Forecasting (ECMWF) and The (United Kingdom) Met Office (MetO) for 1994/1995 and 1995/1996, isolating a warm bias at low temperatures in the Arctic compared to radiosondes. *Knudsen et al.* [2002] compared operational analyses against temperatures measured from Ultra-Long Duration Balloons, finding typical biases of about 1K in the analyses compared to the *in-situ* data. *Pawson et al.* [1999] found that temperature estimates from the Tiros Operational Vertical Sounders (TOVS) data, as retrieved at the MetO [*Bailey et al.*, 1993], were generally warmer than analyses based on radiosondes, although the differences were dependent on the static stability. *Manney et al.* [1996] showed that, in 1991/1992 and 1994/1995, the bias in the National Centers for Environmental Prediction (NCEP) analyses were smaller than those in the MetO analyses. A comprehensive comparison of meteorological analyses from the DAO, ECMWF, MetO and NCEP [*Manney et al.* 2002] revealed quantitative differences that change with time, as the analysis systems and their underlying models are developed.

The present study offers a different type of discussion of the quality of the DAO's analyses. The emphasis of Section 3 is on the different data input into the DAS and the agreement of the analyses with these data, focusing on the thermal structure of the radiosondes and satellite datasets and the contribution of the model. The second part of this study presents a validation of the DAO's forecasts, using the DAO analyses as the reference state. Relatively few studies have examined stratospheric forecasts. *Waugh et al.* [1998] and *Lahoz* [1999] presented statistical analyses of lower stratospheric forecast skill in, respectively, the Global Assimilation and Prediction System (GASP) of the Australian Bureau

of Meteorology and the MetO system. Those studies found that there was considerable day-to-day variability in forecast skill, which depended on the flow regime and its evolution; while the DAO's system shows similar behavior, the focus of the presentation is on the dynamical evolution and physical forcing mechanisms in the model. Earlier works, such as *Simmons and Strüfing* [1983] examined the lower stratosphere in meteorological systems designed primarily for tropospheric forecasting, with an upper boundary near 10hPa. The discussion of Section 4 focusses on two case studies: a highly disturbed flow pattern in late January 2000 and the late winter in March 2000.

The main emphasis of the paper is to examine the roles of the different input datasets and the model on the accuracy of the analyses and forecasts in the winter lower stratosphere. The motivation is that accurate temperature analyses are needed for studies of PSC processing of air masses in the polar vortex. The paper ends with a summary and discussion of the main results, pointing the way for future developments in the DAO's analysis system.

2. The assimilation and forecast system

To support NASA's Earth Observing System (EOS) Terra satellite, in late October 1999 the DAO began operational service with the Goddard Earth Observation System, Version 3 (GEOS-3) data assimilation system (DAS). The major components of this system are summarized by *DAO* [1996], which describes the previous (GEOS-2) system in detail. Several major changes were implemented in the transition from GEOS-2 to GEOS-3. Some of these were in the GEOS model [*Suarez and Takacs,*1995]. The most substantial updates were the inclusion of a complex land-surface model and a moist-turbulence scheme, which led to substantial improvements in the lowermost troposphere and at the land surface. In support of the EOS mission, the horizontal resolution of the GEOS general circulation model was increased from 2.5°×2° (longitude by latitude) to 1°×1°. In the lower stratosphere, the vertical resolution is around 1.5-2

km. The upper boundary of the 48-level model is located at about 0.01~hPa in the mid-mesosphere; even though the model extends well into the mesosphere, this upper region is not accurately analyzed, since no information from TOVS observations is available at pressures lower than 0.4hPa.

The input data include all available "conventional" observations, from the surface network and from aircraft. There are two major sources of input data for the middle atmosphere. The first of these is from the upper-air sounding network; these radiosondes generally reach up to about 50hPa, with strongly decreased coverage near 30hPa and 10hPa. The second are the TOVS satellite data [*Smith et al.* 1979]. TOVS comprises of the High-resolution InfraRed Sounder (HIRS), the Microwave Sounding Unit (MSU) and the Stratospheric Sounding Unit (SSU) data. In the 1999/2000 winter, data from the Nimbus-14 platform were used; pre-retrieved geopotential thickness [e.g., *Schlatter*, 1981] from the National Environmental Satellite Data Information Service (NESDIS) were used. These retrievals are performed using an undisturbed reference temperature profile as the *a-priori*, thus may not respond to the local conditions. In the GEOS DAS, a bias correction is applied [*DAO*, 1996] to these data, to account for some of the bias from radiosonde observations: this is strongest in the tropical tropopause region.

Poleward of 30° in each hemisphere, a mass-wind (geostrophic) balance criterion was applied to relate the geopotential thicknesses to the thermal wind. Different data types are combined using the Physical-space Statistical Analysis Scheme (PSAS: *Cohn et al.* [1998]). Note that the winds and geopotential heights (along with surface pressure and moisture) are combined to produce the fields used in the data assimilation; temperature is not included in the data, but is related to geopotential thickness.

The assimilation process proceeds on a six-hour cycle, with analyses produced at 00, 06, 12, and 18GMT. The GEOS-3 assimilation is performed using the so-

called incremental analysis updates (IAU: *Bloom et al.* [1996]), in which the difference between the observations and the six-hour forecast (the O-F) is determined and used to compute the "missing" forcing which the model requires to agree with the observations; the model is then re-integrated from the previous analysis time using the IAUs for temperature, horizontal winds, surface pressure and moisture as additional forcing terms in the Navier-Stokes Equations. As an example, the thermodynamic energy equation is modified to:

$$T_t = Q + \Delta T_{IAU}, \tag{1}$$

where T is the temperature, the differentiation being the absolute derivative with respect to time, Q is the diabatic heating rate, and ΔT_{IAU} is the "non-physical" forcing. In GEOS-3 the geopotential height, rather than temperature, is analyzed, so ΔT_{IAU} is determined from the O-F of geopotential thickness. The IAU technique avoids "shocking" the model by including (relatively) infrequent data insertions, by smoothing over a six-hour interval; this type of insertion does allow the model to compensate for, or "resist," the forcing. A final point is that the analysis cycles are centered on the analysis times: observations for 12UT are for the 9-15UT window; ΔT_{IAU} is applied to the 9-15UT window, meaning that by 12UT (the analysis time) only half of the IAU forcing has been applied.

The GEOS-3 forecasts begin at 3GMT and 15GMT: unlike the analyses, ΔT_{IAU} is incorporated into the model for six hours, before it runs freely in forecast mode, so that (say) the nominal 24-hour forecast is only 21 hours after ΔT_{IAU} was last applied to the model. The formulation of the DAS precludes experiments into the impact of this, but it is likely to be small. The operational GEOS-3 forecasts have a horizontal resolution of 2.5°×2°; while this is rather low for present-day tropospheric forecasts, it is adequate to provide information about the synoptic scale circulation of the middle atmosphere.

3. Evaluation of the DAS

This section presents an overview of the performance of the DAS. A brief summary of the winter 1999/2000 in the polar stratosphere is followed by an evaluation of the agreement between the analyses with the observations and the impacts of data and the model.

3.1 A brief summary of the winter

Different aspects of the meteorology of the 1999/2000 northern winter are given by *Manney and Sabutis* [2000], who focus on the cold early winter, and *Newman et al.* [2002], who discuss the winter in the context of Solve/Theseo. For reference, a brief summary of the temporal evolution of the lower stratosphere in the DAO analyses is provided by Fig. 1, which shows 50-hPa time series of North-Pole temperature and the zonal-mean zonal wind at 60°N. The evolution of the winter is characterized by decreasing temperature in November before a strong disturbance evolved, warming the polar cap and reducing the jet strength in the latter half of November and early December. After the decay of this disturbance, low temperatures were reached by late December. These persisted until a minor warming perturbed the flow in February, but in the second half of the month temperatures again fell below 195K. March was dominated by a series of warmings that slowly increased the temperature, but the final wind reversal did not occur until well into April.

Synoptic maps illustrate the differing character of the flow throughout the winter. Of particular interest to this study is the structure in late January, when the flow pattern was very distorted and the coldest region in the low stratosphere was displaced towards Scandinavia (Figure 2). The pronounced "wavenumber 3" structure that dominated the stratospheric flow was associated with a blocking pattern in the troposphere, with a pronounced ridge over the northern Atlantic and the North Sea and a trough extending from the polar region through

Scandinavia and Russia. The pronounced zonal asymmetry has a similar structure throughout the troposphere and lower stratosphere over the region between North America to central Russia (Fig. 2). This circulation pattern was important to the Solve/Theseo mission, since cold, vortex-core air over Kiruna was transported from the polar night into illuminated regions, potentially allowing the processing of polar air masses. Accurate forecasts of this flow structure were important for aircraft- and balloon-flight planning in Solve-Theseo. The accuracy of the GEOS-3 analyses and forecasts during this event will be discussed.

3.2 Data impacts

There are two primary types of observations in the high-latitude lower stratosphere. These are: (i) the upper-air sounding network, with a sparse distribution at the highest latitudes, which is referred to as the SONDE dataset, and (ii) the NESDIS (National Environmental Satellite Data Information Service) retrievals of TOVS data. The impacts of the datasets, as well as the differences between them, are discussed here. Note that commercial aircraft flight-path data, which are used in the analyses, can also impact the lower stratosphere, but these are generally outside the region of interest for this study. The discussion of the SONDE and TOVS data is limited to the region poleward of 50°N.

The total number of sonde observations at 50hPa in January 2000 (Fig. 3a) illustrates: (i) the high density of daily and twice daily soundings at isolated locations over Europe and North America (more that 30 or 60 soundings in the month); (ii) the sub-daily reports over much of Russia; (iii) sparse data over some oceans; and, (iv) no upper air soundings poleward of 75°N. Note that all data in this discussion are presented as values on a 1° ×1° grid, with each sonde located in the analysis grid box in which it falls. The satellite orbit and viewing geometry result in a more uniform spatial coverage for the TOVS data (Fig. 3b), with fewer (about five to ten) observations per grid box over middle latitudes and just one or two observations in the month over the Arctic Ocean (note that the six-hour

analysis cycle means that there are a total of 124 analysis times in January 2000).

The discussion is centered on the so-called "observation minus analysis" (O-A) field for the geopotential height (Z), for both the SONDE and TOVS datasets. To distinguish between the data sources and the variables, the (O-A) values are denoted ($Z_{TOVS} - Z$) and ($Z_{SONDE} - Z$), where the absence of a subscript denotes the analyzed value and subscripts denote the data source. (Equivalent notation will be used for temperature.) Figure 4 shows the areal averages of these fields for the 50°N-70°N and 71°N -90°N. In the polar region there are almost no sonde observations, so that ($Z_{TOVS} - Z$) arises from the imbalance between the model and the retrieved TOVS data. Below 70hPa, the bias is positive and increasing with altitude, meaning that the analyses are cooler than the NESDIS-TOVS observations; in the stratosphere, this relationship reverses.

For the 50°N-70°N region, the situation is more complex, because both types of observations exist. Between about 700 and 70hPa, ($Z_{SONDE} - Z$) is negative and slightly decreasing, while ($Z_{TOVS} - Z$) is positive and, between 300 and 70hPa, increasing rapidly (it is similar to the polar-cap profile). When subsampled only at the points coincident with SONDE observations, the relative bias in the NESDIS-TOVS data almost doubles at 70hPa. (In this study, coincidence means within the same 1° ×1° grid box and the same six-hour interval: these values are dictated by the analysis system.) This large increase with altitude below 70hPa of ($Z_{TOVS} - Z$) corresponds to a warm bias in the NESDIS-TOVS data compared to both the SONDE data and the analyses. In this lowest part of the stratosphere, the analyses are only slightly cooler than the SONDE observations. Between 70 and 30hPa, the signs of the thermal bias are reversed, as the TOVS height bias reduces rapidly from a maximum of about 22gpm to a value close to 6gpm.

Since geopotential height, rather than temperature, is assimilated in GEOS-3, all monitoring is based on Z. However, a consistent discussion of thermal structure

can be developed by reference to the layer-mean temperature ($\check{T}$), determined from the geopotential thickness. Since the main focus of this work is on the temperature, this approach is adopted. Figure 5 shows the zonal-mean difference in $\check{T}$ between the two data types and the GEOS-3 analyses, denoted as ($\check{T}_{SONDE}$ - $\check{T}$) and ($\check{T}_{TOVS}$ - $\check{T}$), for two stratospheric layers (50-30hPa and 150-100hPa), selected to highlight the height regions with different relative biases. These illustrate that the latitudinal structure of the biases are almost reversed at the two altitudes, have opposite signs for the two data types, and are smaller for the SONDE dataset: these last two aspects reflect the weightings given to the two data types in the analysis. Reducing the TOVS sampling to only the times and locations with a coincident radiosonde observation leads to substantial increases in ($\check{T}_{TOVS}$ - $\check{T}$). A similar co-location filter for the SONDE data has a smaller impact.

The geographical distribution of (O-A) is also of interest. Results for the 30-50hPa and the 100-150hPa layers are presented (Plates 1 and 2). The January-2000 average of $\check{T}$ is shown in these plots, highlighting the cold pool displaced towards Scandinavia, with much higher temperatures in the Pacific sector. There is a temporal and spatial inhomogeneity in the sampling at different grid points (Fig. 3). For the 30-50hPa layer, ($\check{T}_{SONDE}$ - $\check{T}$) is generally positive (Plate 1), consistent with the zonal-mean results in Fig. 5, although several stations in all parts of the globe show weak, negative values. At this level, ($\check{T}_{TOVS}$ - $\check{T}$) shows fairly strong negative biases over Europe and North America and Asia, where there are Sonde data, but is positive over large regions of the oceans. For the 100-150hPa layer, the signs of the biases for ($\check{T}_{TOVS}$ - $\check{T}$) are reversed, and the land-ocean contrast remains. At this lower level, the bias in ($\check{T}_{SONDE}$ - $\check{T}$) is smaller than in the 30-50hPa layer, scattered each side of the zero line. This explains the smaller differences in the zonal-mean (Figure 5). Of note are the additional coneventional observations over the North Atlantic (mainly aircraft flight paths, which are grouped with the SONDE data), most of which show a weak bias.

These results indicate that the bias (relative to the analyses) of the SONDE data is smaller than that of the TOVS data. The analysis is correctly drawn to the SONDE data, but the existence of land-sea contrasts in the TOVS bias suggests that the analyses are impacted by the uneven spatial coverage of the sonde data. The $(\check{T}_{TOVS} - \check{T})$ biases have a pronounced vertical structure, which will impact the analyses.

3.3 Analysis increments and forcing

As summarized in Section 2, the (O-F) fields are used to build the IAU forcing terms, which are applied to the GEOS-3 model. In the extratropics, the additional forcing applied to wind and the thermal structure is balanced. The zonal-mean of ΔT_{IAU} (see Eq. 1) is compared to the diabatic tendencies (Q in Eq. (1)) in Fig. 6. This shows that the observations require a warming of the middle troposphere (700-500hPa, slightly higher in middle latitudes) and a cooling above this. In the polar region, ΔT_{IAU} is positive in the layer between 200 and 100hPa, but it is stronger and negative aloft. This vertical structure is consistent with the (O-A) fields discussed in Section 3.2. For comparison, the zonal-mean of Q calculated from the model shows diabatic cooling almost everywhere, with smaller magnitude in the polar lower stratosphere than in the upper troposphere and middle stratosphere. It is of significance that ΔT_{IAU} (the non-physical cooling required to force the model towards the observations) is comparable in many regions to the modeled diabatic cooling. This indicates a substantial bias in the model, with either too little diabatic cooling (from the parameterized physics) or too much adiabatic warming from dynamical processes. In the stratosphere, such a large correction indicates that the data insertion is forcing the model to depart from its radiative-dynamical balance, implying a bias in the model circulation.

The spatial structure of ΔT_{IAU} at 50hPa and 150hPa (Fig. 7) has a pronounced zonal asymmetry, resembling the (O-A) fields in Plates 1 and 2. The forcing acts

to extend the coolest part of the vortex over Southern Greenland, Northern Scandinavia and Russia, and over Western Siberia, while adding heat over most of northern Canada, the North Sea, and Central Siberia. These is some vertical structure in ΔT_{IAU}, especially over the North Sea and northern Russia, which can also be related to the differences in the (O-A) fields at the two levels.

4. Evaluation of the GEOS-3 forecasts

The results presented in this section are intended to give an overview of the large-scale performance of the DAO's forecasts in the Solve/Theseo winter. A case study is presented to illustrate the performance of the forecasts in late January 2000, when the strong wavenumber-3 pattern dominated the lower stratospheric flow (Figure 2). A second case study examines the fields in late winter. Following this, some more specific results concerning the forecasting of cold regions, where polar stratospheric clouds (PSCs) might form, are discussed.

4.1. Case study: late January 2000

The latter part of January 2000 was dominated by the blocking pattern, which distorted the polar vortex in the lower stratosphere (Fig. 2). The period January 21-30, 2000, was selected for detailed analysis, because of the importance of this flow pattern to PSC processing of air masses and because of the anomalous nature of the flow. The temperature biases of the 5-day forecasts at 50hPa (Fig. 8) show the tendency of the model to reduce the zonal asymmetry of the flow. The southern extremities of the region colder than 200K over both Europe and North America show warm biases of more than 6K, while the warmer region over eastern Siberia and Alaska is more than 12K too cold in the five-day forecasts. The vertical structure of the zonal temperature anomaly at 60°N (Fig. 9) reiterates the strong temperature anomalies throughout the troposphere and stratosphere over this 10-day period, with a typical pronounced westward tilt leading to a strong northward eddy heat transport near the tropopause, which

peaks at about 24Km/s at 60°N (Fig. 10). The five-day forecast fields show a much reduced eddy pattern (Fig. 9): the main feature of the forecast is a suppression of the "wavenumber-2" component of the flow, a pattern which persists throughout the troposphere and stratosphere. The reduction in strength of the zonally asymmetric component of the flow causes a decrease (of more than half) in the eddy heat flux through the lower stratosphere (Fig. 10) and an increase in the strength (from about 46 to 53 m/s) and a narrowing of the polar night jet (Fig. 11) in the five-day forecast. These changes are consistent in the diagnostic framework of the mean meridional circulation: underestimated eddy amplitudes in the troposphere reduce the eddy forcing of the middle atmosphere, leading to a stronger jet. However, such diagnostic arguments do not adequately address causality. The vertical coherence of the five-day forecast bias suggests that the model is unable to support the strong blocking event and, hence, unable to represent its effects on the temperature of the lower stratosphere: this suggests that the circulation ought to be considered more in terms of the local features, which are being suppressed in the model. The tendency of the model to underestimate the effects of the zonal asymmetries are consistent with multi-year simulations, since *Pawson et al.* [2000] found that the GEOS-2 model (with an almost identical middle atmosphere) did not capture an adequate Aleutian high; however, the same study showed an underestimate in jet strength in the lower stratosphere. These apparent inconsistencies presumably arise from the different timescales (multi-annual and five-day simulations), as well as the highly disturbed flow field in late January 2000.

These medium-range forecasts for January 21-30, 2000 are consistent with the analysis increments and the IAU forcing applied to the model to correct for forecast bias in the analyses. This implies that the five-day forecasts show biases qualitatively similar to the initial (six-hour) tendencies in the model, emphasizing the importance of the model performance to the quality of the analyses as well as the forecasts.

4.2. Case Study: March 2000

The late winter and spring is a period of change in the middle atmosphere, as the polar vortex breaks and the flow transitions to a summertime pattern with easterlies. In March 2000, the vortex remained but was much weaker than in January and February. The GEOS-3 analyses show a monthly average temperature of 210K, displaced towards Scandiavia, with much warmer values elsewhere (Fig. 12). As in late January, the five-day forecasts tend to underestimate the zonal asymmetries of the flow, although in this case the bias peaks at about 3K (both the longer averaging period and the less distorted flow field contribute to this). The differences (Fig. 12) clearly show that the model tends to suppress the development of the cold region over Scandinavia and to pull the warm region back towards the Pole. The polar night jet (not shown) peaks at about 15m/s in the March average, and is overestimated by about 3m/s in the five-day forecast. Even though the dynamical regime in March is very different from that in late January, the model biases are similar: the zonal-mean structure is too pronounced and eddies are suppressed at all levels. The issues of model bias, as revealed by comparing the thermal forcing terms, are also similar to in the middle winter: both Q and ΔT_{IAU} show cooling in the middle stratosphere in the polar region, where the physical tendencies are considerably larger than the analysis forcing. Near 100hPa, a sizable warming tendency (ΔT_{IAU} = 1.5K/day) is applied in a region where Q is weak and negative; near 300hPa, a layer with very weak diabatic cooling shows a pronounced maximum in ΔT_{IAU}. Again, even though the dynamical regime and radiative forcing are very different in March than in January, there are considerable biases between the model and the observations.

4.3. Meteorological measures of forecast bias

A quantity of particular relevance to lower stratospheric chemistry is the area covered by low temperature, which impacts the likely exposure of polar air

masses to polar stratospheric cloud formation and subsequent denitrification [e.g., *Newman et al.*, 1990; *Pawson et al.*, 1995]. At 50hPa, a typical temperature for PSC formation is 195K, while ice clouds form near 188K. Time series of A_T the area colder than temperature T, are shown for five values of T (ranging from 190K to 210K) in Plate 3a. With some exceptions (e.g., January 13), A_T is underpredicted by the 5-day forecasts, often by at least 10% of the analyzed value. From a slightly different perspective, Plate 3b shows the temperature bias of the five-day forecasts for regions where the analyzed temperature was below the same five values. In the coldest part of the winter, these show a cold bias at all temperatures, which ranges from about 1K for T = 210K and can reach 6K for T = 195K (where A_T is small). The forecast bias in these cold regions was largest when the vortex was disturbed: in November and in late January and early February. At these times, standard statistical measures of forecast skill (such as bias and anomaly correlation) were also lower than for the undisturbed periods.

5. Discussion and conclusions

An analysis of the performance of the DAO's meteorological analyses and forecasts for the Solve/Theseo period has been presented. The GEOS-3 system, with which these products were produced, has been operational in the DAO since November 1999.

The two main data types for the middle atmosphere are the radiosonde network and the TOVS satellites. These have quite different spatial and temporal sampling characteristics, as well as different accuracies. The large-scale signature of the TOVS data can be seen in the incremental forcing which is applied to the model in order to force it towards observations. The sparsity of the radiosonde observations means that they can only have a localized impact on the analyses, which is also evident in the forcing increments. One of the most

challenging aspects of assimilating these different data types in the large bias between them, which is particularly strong between 300 and 70hPa: the NESDIS retrievals of TOVS data are much warmer than the sondes in the very low stratosphere, but cooler than the sondes above this. In terms of obtaining accurate analyses for calculations PSC formation, this offers particularly strong challenges. The absence of sonde observations over large parts of the hemisphere means that weight can only be given to the TOVS data and the model there; air which then flows into a region with sonde observations will necessarily have a biased temperature compared to the sondes. These differences between the input data could partly arise from the retrievals of the TOVS data; a new, radiance-based analysis system [*Joiner and Rocke*, 1999] is being implemented in the DAO's GEOS-4 analysis system. This allows a much more consistent treatment of the radiances in terms of local conditions.

The impact of model/observation bias is also apparent in the analyses and analysis increments. The fact that the additional (IAU) cooling is of comparable strength to the diabatic cooling in the model is particularly worrisome. This points to deficiencies in the model circulation, the physical packages, or both. If the cause were radiative, the most likely reasons for the large model bias would be deficient calculations of radiative heating and cooling rates, arising either from the radiation scheme or from the ozone climatology, which is a specified, zonal-mean product. Steps are presently being taken to couple the DAO's ozone assimilation system [*Štajner et al.*, 2001] with the meteorological system, so that consistent ozone distributions can be used at any time.

However, the five-day forecasts and the magnitude of the IAU forcing point to the prime cause of the model-analysis biases as being dynamical, rather than from missing physical processes. The main argument in support of this is the strong zonal asymmetry and the rapid growth of the biases: in late January the biases occur in relationship to the flow and on a timescale (growing more than 10K in the five-day forecast) much to rapid to be caused by a radiation problem (since

radiative relaxation timescales in the lower stratosphere are on the order of tens of days). The GEOS-3 model tends to suppress zonal anomalies, cannot represent very cold features in the lower stratosphere, and on the timescales discussed here, it supports an over-zonal flow.

This study has identified and discussed some of the most important aspects of the DAO's GEOS-3 data assimilation system. Studies such as *Manney et al.* [2002] that provide quantitative measures of several analysis systems play an important role in determining the relative performance of products from different centers. Detailed comparisons of analyzed datasets with independent, *in-situ* measurements [e.g., *Knudsen et al.*, 2002] are important in establishing a ground truth, which is particularly critical for studies of polar processing. The work presented in this paper has been directed more at the different factors impacting a single analysis system: it has been shown how relative biases between different input datasets (in this case, sonde and NESDIS-TOVS data) affect the analyses, and how the model has clear deficiencies that must be corrected.

The calculations presented here are a benchmark for monitoring and evaluation of the DAO's operational system. Present research in the DAO involves testing the GEOS-4 system, which contains several major updates, not least an entirely different circulation model and the elimination of the IAU concept, as well as the radiance-based assimilation of TOVS data. A priority of DAO research is to reduce the systematic deficiencies of the GEOS-3 system that have been identified here. The results of the present study suggest that particular sensitivity calculations, such as examination of the causes of deficiencies in the model and their impacts on the analyses and forecasts are necessary. Because of the transition to GEOS-4, no such studies have been performed for this work. However, a similar evaluation of GEOS-4 is underway, and the results will be used to guide a set of quantitative experiments using that system. While the formulation of GEOS-4 is vastly different from GEOS-3, meaning that the nature of the model and the data types will change, the present results highlight the

types of imbalance between model and data that are inherent in the field of data assimilation.

Acknowledgements

We are grateful to colleagues in the DAO for assistance with the data handling and computing which are essential for the DAS to be run operationally. We thank Dick Dee, Ricardo Todling and Arlindo da Silva for their patient explanations of the analyses and Steve Bloom for the inspiration to look carefully at the data. Gloria Manney made helpful comments on an early version of the manuscript.

References

Bailey, M.J., A. O'Neill, and V.D. Pope, 1993: Stratospheric Analyses Produced by the United Kingdom Meteorological Office. *J. Appl. Meteorol.*, **32**, 1472-1483.

Bloom, S.C., L.L. Takacs, A.M. da Silva and D. Ledvina,1996: Data Assimilation Using Incremental Analysis Updates. *Mon. Weath. Rev.*, **124**, 1256-1271.

Burris, J., T. McGee, W. Hoegy, L. Lait, L. Twigg, G. Sumnicht, W. Heaps, C. Hostelter, T.P. Bui, R. Neuber, and I.S. McDermid, 2002: Validation of Temperature Measurements from the Airborne Raman Ozone, Temperature and Aerosol Lidar During Solve. *J. Geophys. Res.*, in press.

Cohn, S.E., A. da Silva, J. Guo, M. Sienkiewicz, and D. Lamich, 1998: Assessing the Effects of Data Selection with the DAO Physical-Space Statistical Analysis System. *Mon. Weath. Rev.*, **126**, 2913-2926.

Coy, L. and R. Swinbank, 1997: Characteristics of Stratospheric Winds and Temperatures Produced by Data Assimilation. *J. Geophys. Res.*, **102**, 25,763-25,781.

DAO, 1996: Algorithm and Theoretical Basis Document for Goddard Earth Observing System Data Assimilation System (GEOS DAS) With a Focus on Version 2. Data Assimilation Office, NASA's Goddard Space Flight Center, 310pp.

Joiner, J., and L. Rokke, 2000: Variational Cloud Clearing with TOVS Data. *Q. J. R. Meteorol. Soc.*, **126**, 725-748.

Knudsen, B.M., 1996: Accuracy of Arctic Stratospheric Temperature Analyses and the Implications for the Prediction of Polar Stratospheric Clouds. *Geophys. Res. Lett.*, **23** 3747-3750.

Knudsen, B.M., J.-P. Pommereau, A. Garnier, M. Nunes-pinharanda, L. Denis, P.A. Newman, G. Letrenne, and M. Durand, 2002: Accuracy of Analyzed Stratospheric Temperatures in the Winter Arctic Vortex from Infrared Montgolfier Long-Duration Balloon Flights. Part II: Results. *J. Geophys. Res.*, in press.

Lahoz, W.A., 1999: Predictive Skill of the UKMO Unified Model in the Lower Stratosphere. *Quart. J. R. Meteorol. Soc.*, **125**, 2205-2238.

Manney, G.L., and J.L. Sabutis, 2000: Development of the Polar Vortex in the 1999/2000 Arctic Winter Stratosphere. *Geophys. Res. Lett.*, **27**, 2589-2592.

Manney, G.L., R. Swinbank, S.T. Massie, M.E. Gelman, A.J. Miller, R. Nagatani, A. O'Neill and R. Zurek, 1996: Comparison of U.K. Meteorological Office and U.S. National Meteorological Center Stratospheric Analyses During Northern and Southern Winter. *J. Geophys. Res.*, **101**, 10,311-10,334.

Manney, G.L., J.L. Sabutis, S. Pawson, M.L. Santee, B. Naujokat, R. Swinbank, M.E. Gelman, and W. Ebisuzaki, 2002: Lower Stratospheric Temperature Differences Between Meteorological Analyses in Two Cold Arctic Winters and their Impact on Polar Processing Studies. *J. Geophys. Res.*, in press.

Newman, P.A., L.R. Lait, M.R. Schoeberl, and R.M. Nagatani, 1990: Stratospheric Temperature During the 88--89 Northern Hemispheric Winter. *Geophys. Res. Lett.*, **17**, 329--332.

Newman P.A., N.R.P. Harris, A. Adriani, G.T. Amanatidis, J.G. Anderson, G.O. Braathen, W.H. Brune, K.S. Carslaw, M.T. Craig, P.E. DeCola, M. Guirlet, S.R.

Hipskind, M.J. Kurylo, H. Kuellmann, N. Larsen, G.J. Megie, J.-P. Pommereau, L.R. Poole, M.R. Schoeberl, F. Stroh, O.B. Toon, C.R. Trepte, and M. van Roozendael, 2002: An Overview of the SOLVE-THESEO 2000 Campaign. *J. Geophys. Res.*, in press.

Pawson S. and B. Naujokat, 1999: The Cold Winters of the Middle 1990s in the Northern Lower Stratosphere. *J. Geophys. Res.*, **104**, 14,209--14,222.

Pawson S., B. Naujokat, and K. Labitzke, 1995: On the Polar Stratospheric Cloud Formation Potential of the Northern Stratosphere. *J. Geophys. Res.*, **100**, 23,215-23,225.

Pawson, S., K. Krueger, R. Swinbank, M. Bailey and A. O'Neill, 1999: Intercomparison of Two Stratospheric Analyses: Temperatures Relevant to Polar Stratospheric Cloud Formation. *J. Geophys. Res.*, **104**, 2041-2050.

Schlatter, T.W., 1981: An Assessment of Operational TIROS-N Temperature Retrievals over the United States. *Mon. Weath. Rev.*, **109**, 110-119.

Schubert, S.D., R.B. Rood, and J. Pfaentner, 1993: An Assimilated Dataset for Earth Science Applications. *Bull. Am. Meteorol. Soc.*, **74**, 2331-2342.

Simmons, A.J., and R. Struefing, 1983: Numerical Forecasts of Stratospheric Warmings Using a Model with a Hybrid Vertical Coordinate System. *Quart. J. R. Meteorol. Soc.*, **109**, 81-111.

Smith, W.L., H.M. Woolf, C.M. Hayden, D.Q. Wark, and L.M. McMillan, 1979: The TIROS-N Operational Vertical Sounder. *Bull. Am. Meteorol. Soc.*, **60**, 1177-1187.

Štajner, I., L.P. Riishogjaard, and R.B. Rood, 2001: The GEOS Ozone Data Assimilation System: Specification of Error Statistics. *Q. J. R. Meteorol. Soc.*, **127**, 1069-1094.

Suarez, M.J. and L.L. Takacs, 1995: Documentation of the Aries/GEOS Dynamical Core: Version 2. NASA Tech Memo 104606, Vol. 5, NASA Goddard Space Flight Center, Greenbelt, MD, 45pp.

Swinbank, R., and A. O'Neill, 1994: A Stratosphere-Troposphere Data Assimilation System. *Mon. Weath. Rev.*, **122**, 686-702.

Waugh, D.W., Sisson, J.M. , and D.J. Karoly, 1998: Predictive Skill of a NWP Model in the Southern Lower Stratosphere. *Quart. J. R. Meteorol. Soc.*, **124**, 2181--2200.

Figure Captions

Figure 1. Time series (November 1, 1999, until March 31, 2000) of T at the North Pole and u at 60°N, determined from DAO analyses. The temperature is shown at 50hPa, while wind is shown at 50hPa (solid) and 10hPa (dotted).

Figure 2. These polar stereographic projections show the geopotential height (gpdm: contours) and temperature (K: shaded) analyses, poleward of 50°N, at 50hPa (top) and 500hPa (bottom). The shading is such that dark tones indicate low temperatures.

Figure 3. These polar stereographic projections, for latitudes poleward of 50°N, show the number of lower stratospheric observations in January 2000. For each one-degree grid box, the total number of observations for the month is given for (a) SONDE and (b) TOVS data.

Figure 4. These curves show the altitude dependence of the areal average of the (O-A) for geopotential height for (left) 50°N –70°N and (right) 71°N –90°N. On the left-hand panel, $(Z_{SONDE} - Z)$ determined from all points with a sonde observation (solid line, with circles) and the subsample from locations with a coincident TOVS observation (dotted line, with circles) are shown, along with the equivalent values from TOVS data (solid/dotted lines, no circles). Since there are almost no SONDE data poleward of 70°N, the only curve on the right-hand panel is for $(Z_{TOVS} - Z)$.

Figure 5. The zonal-means of (O-A) for the layer-mean temperatures ($\check{T}$) for the 50-30hPa (top) and 150-100hPa layers are shown. As in Fig. 4, solid lines denote the means at all points, while dotted lines indicate the values sub-sampled at locations with the other data type, and the curves with circles are for $(\check{T}_{SONDE} - \check{T})$.

Plate 1. This plate gives information about the layer-mean temperature for the 30-50hPa layer. The analyzed mean temperature is illustrated by the contours on both panels, while panel (a) shows ($\check{T}_{SONDE} - \check{T}$) and panel (b) shows ($\check{T}_{TOVS} - \check{T}$), shaded according to the color bar (blue regions indicate where the observations are colder than the analyses. The polar stereographic projections extend from 50°N to the Pole.

Plate 2. As in Plate 1, but for the 100-150hPa layer.

Figure 6. These panels show the zonal-mean "diabatic" forcing in the GEOS-3 model used to produce the analyses. The upper panel shows the physical tendency (Q) from the model parameterizations, while the lower panel shows ΔT_{IAU}. In both panels the contour interval is 0.25K/day and regions with cooling are shaded.

Figure 7. These polar stereographic plots, for latitudes poleward of 50°N, show ΔT_{IAU} at 50hPa (top) and 150hPa (bottom) for January 2000. The contour interval is 0.25K/day and shading denotes negative values.

Figure 8. This plot shows the mean bias between the analysis and the five-day forecast of temperature [K] at 50hPa for the period January 21-30, 2000. It is a polar stereographic projection for the region between 50°N and the Pole. Regions of negative bias (when the forecast is too warm) are shaded and the contour interval is 2.5K. The mean analysis for this period is shown in Fig. 2.

Figure 9. These longitude-pressure sections show the zonal anomaly of temperature [K] (top) and the five-day forecast bias (bottom) at 60°N for the period 20-30 January 2000. Negative values in the lower panel indicate a warm bias in the forecast.

Figure 10. The 100-hPa eddy heat flux [Km/s] is shown for the analyses (solid line) and the five-day forecasts (dotted line) for the extratropical northern hemisphere. These are calculated from the instantaneous velocity and temperature fields for each analysis time between January 21 and January 30, 2000 (i.e., they include contributions from stationary and transient eddies).

Figure 11. These plots show latitude-height sections of the zonal-mean zonal velocity [m/s] and its bias for the period January 21-30, 2000. (a) The mean of the GEOS-3 analyses. (b) The mean difference between the five-day forecasts and the analyses; negative values (shaded) are where the winds in the forecast are stronger than those in the analyses.

Figure 12. These time series, from Nov. 1, 1999, through April 1, 2000, show the underestimation of cold regions in the 5-day forecasts. Panel (a) shows the analyzed (thick) and 5-day forecast (thin) lines of A_{210}, A_{205}, A_{200}, A_{195}, and A_{190}, expressed as a percentage of the area of the northern hemisphere. Panel (b) shows the forecast bias for areas with analyzed temperatures lower than 205K and 195K.

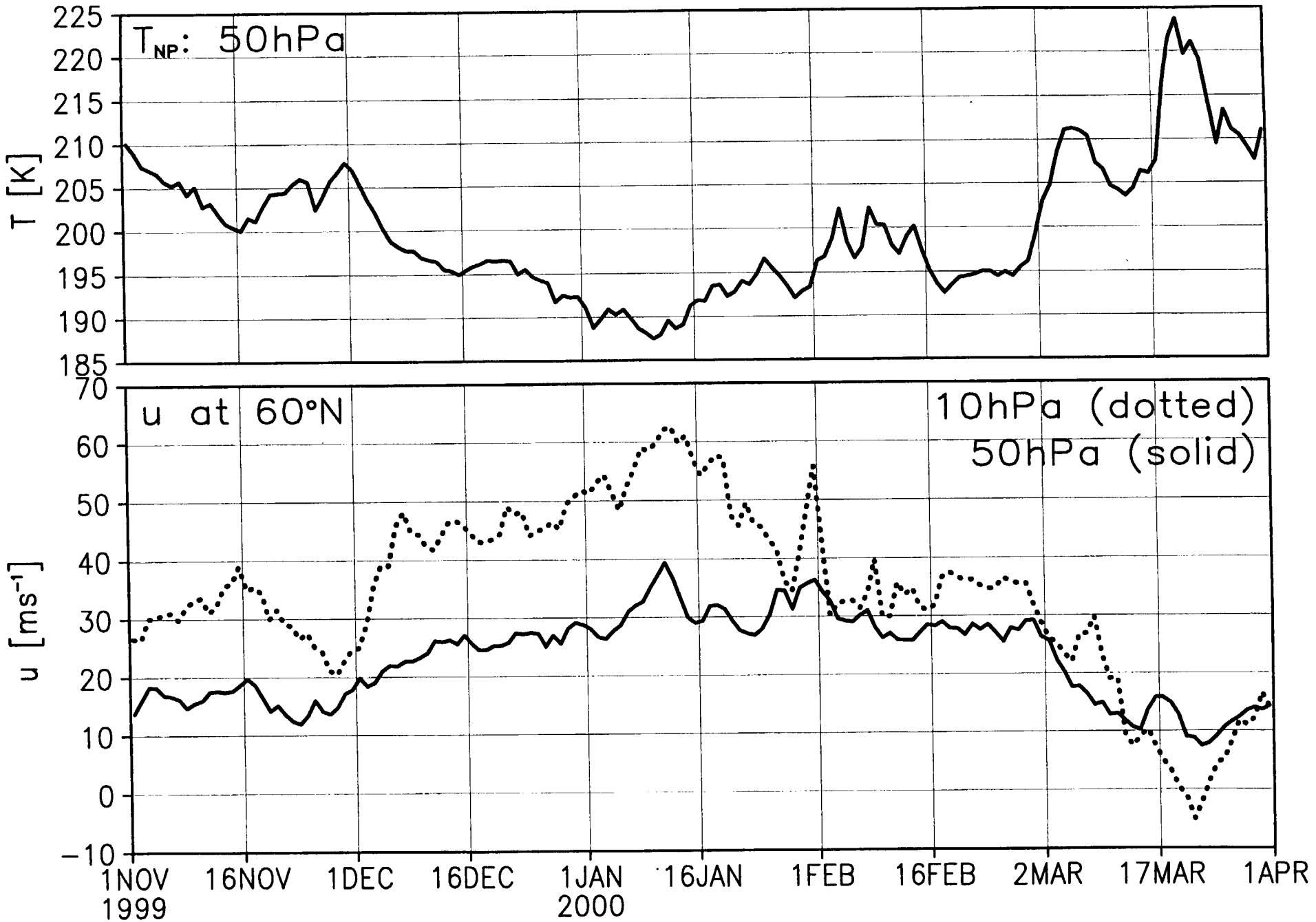
T_{NP}: 50hPa
T [K]
225
220
215
210
205
200
195
190
185
u at 60°N
10hPa (dotted)
50hPa (solid)
u [ms^{-1}]
70
60
50
40
30
20
10
0
−10
1NOV 1999
16NOV
1DEC
16DEC
1JAN 2000
16JAN
1FEB
16FEB
2MAR
17MAR
1APR

Fig 1

Fig 2a

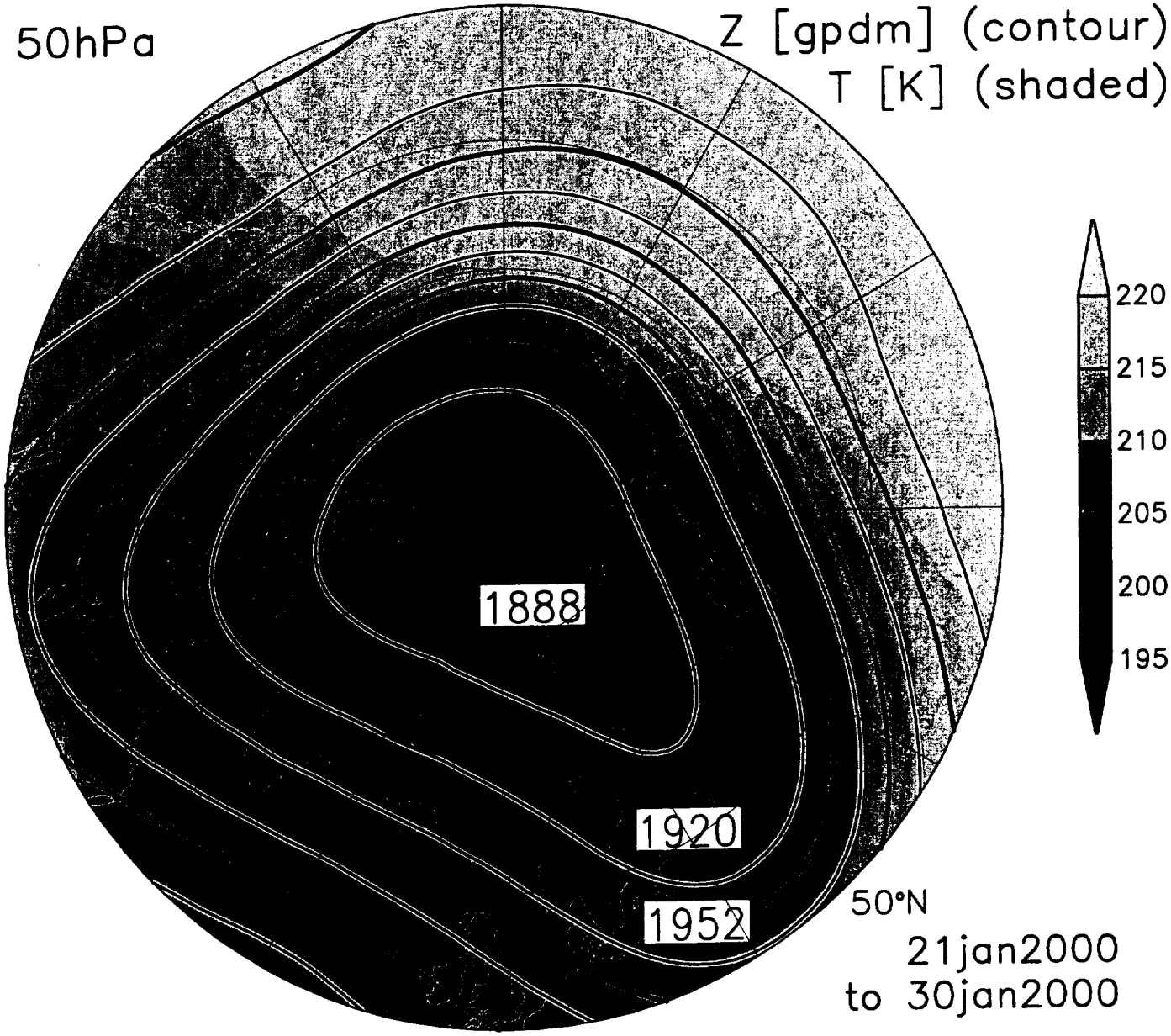
50hPa
Z [gpdm] (contour)
T [K] (shaded)
220
215
210
205
200
195
1888
1920
1952
50°N
21jan2000
to 30jan2000

Fig 2b

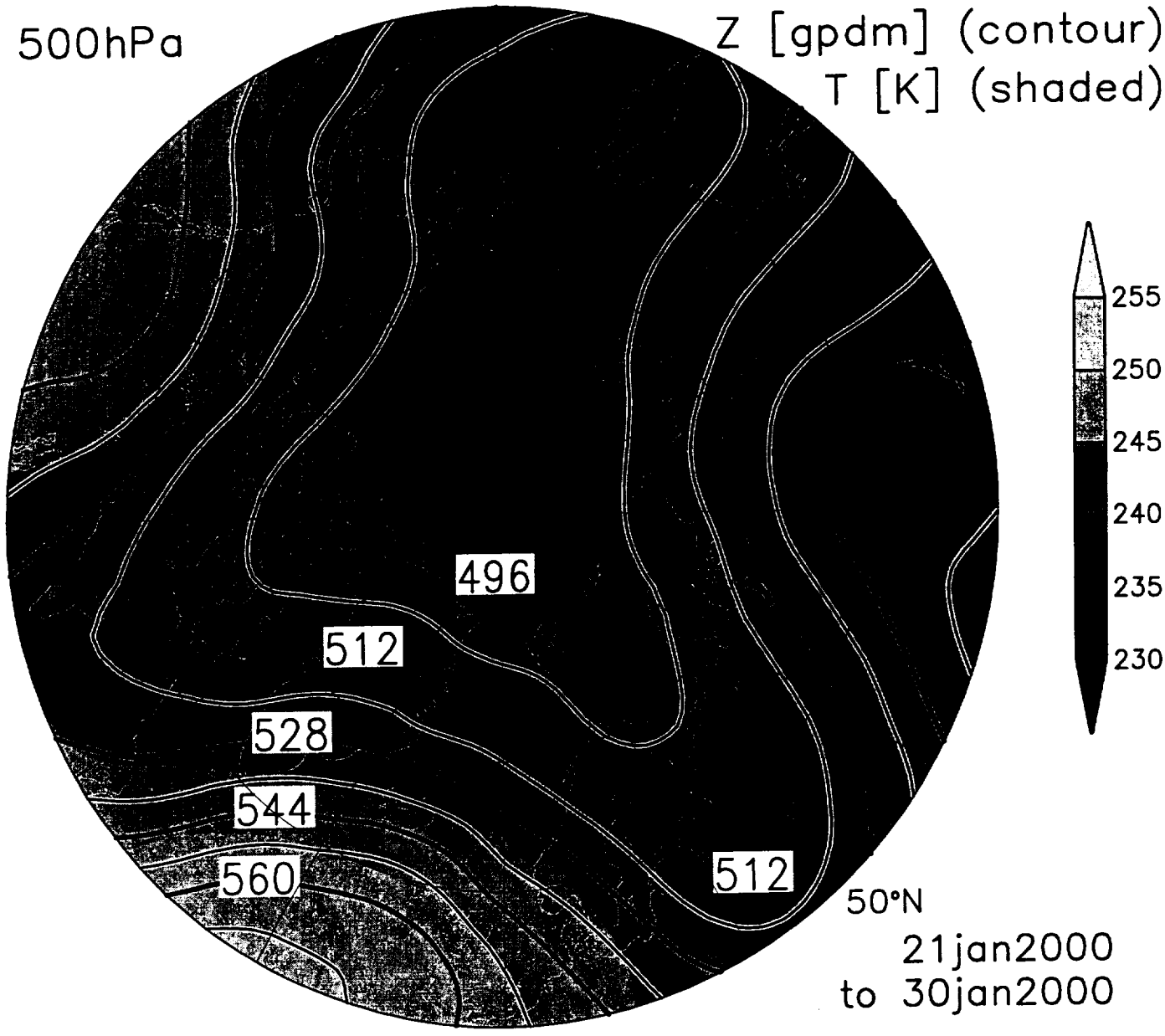
500hPa
Z [gpdm] (contour)
T [K] (shaded)
496
512
528
544
560
512
255
250
245
240
235
230
50°N
21jan2000
to 30jan2000

Fig 3

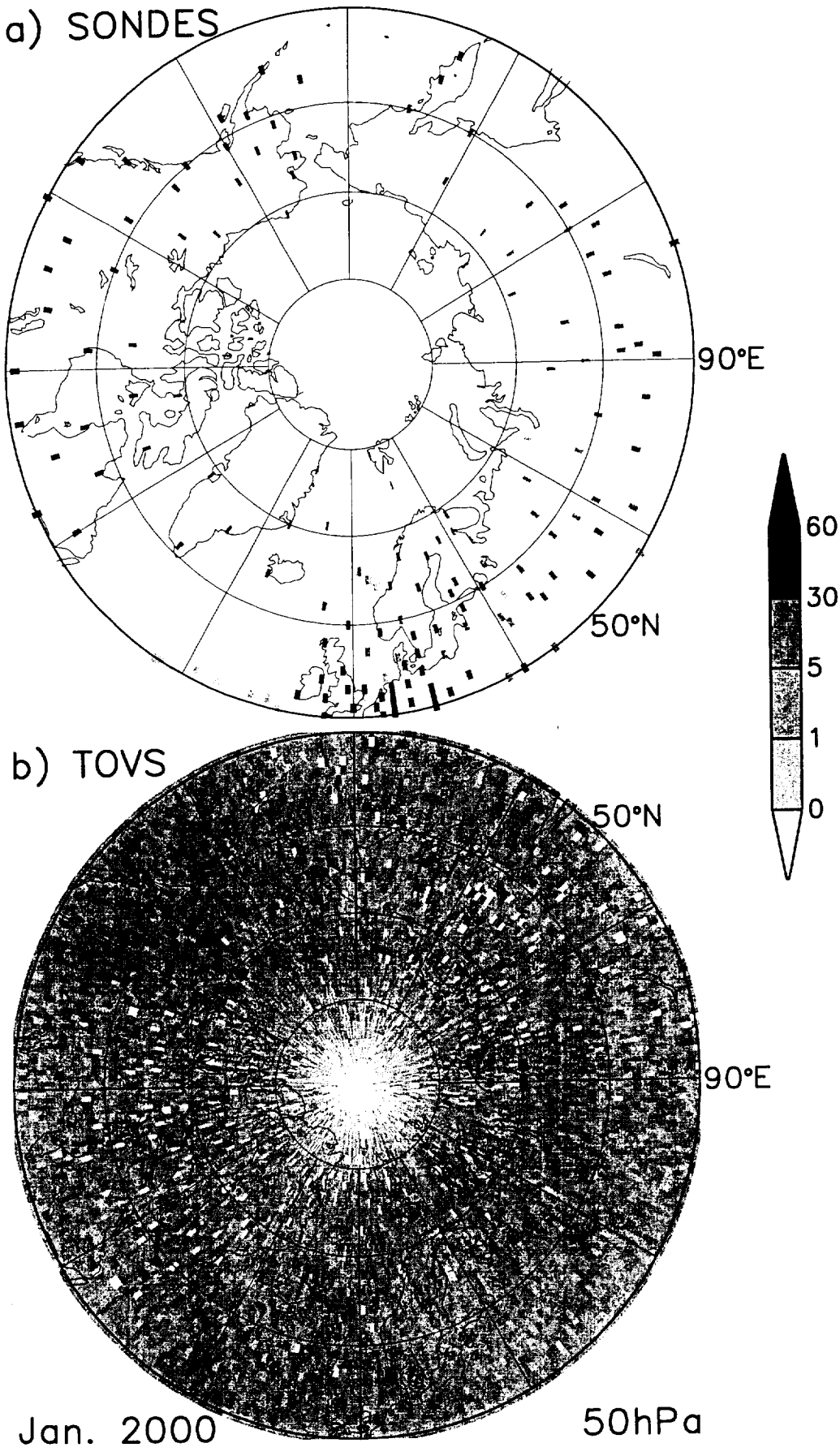

Fig 4

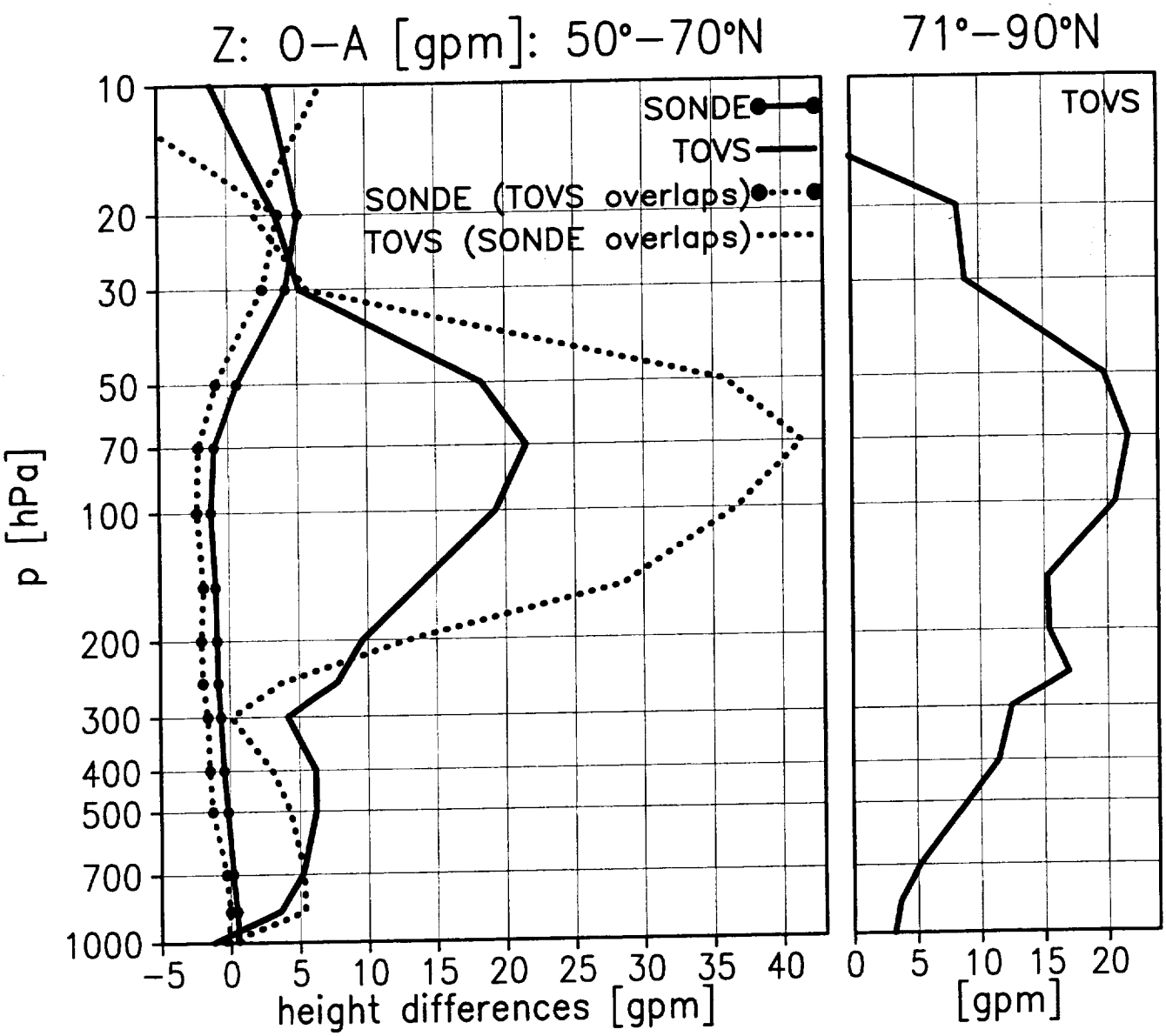
Z: O−A [gpm]: 50°−70°N
71°−90°N
SONDE
TOVS
SONDE (TOVS overlaps)
TOVS (SONDE overlaps)
TOVS
p [hPa]
10
20
30
50
70
100
200
300
400
500
700
1000
−5 0 5 10 15 20 25 30 35 40
height differences [gpm]
0 5 10 15 20
[gpm]

Fig 5

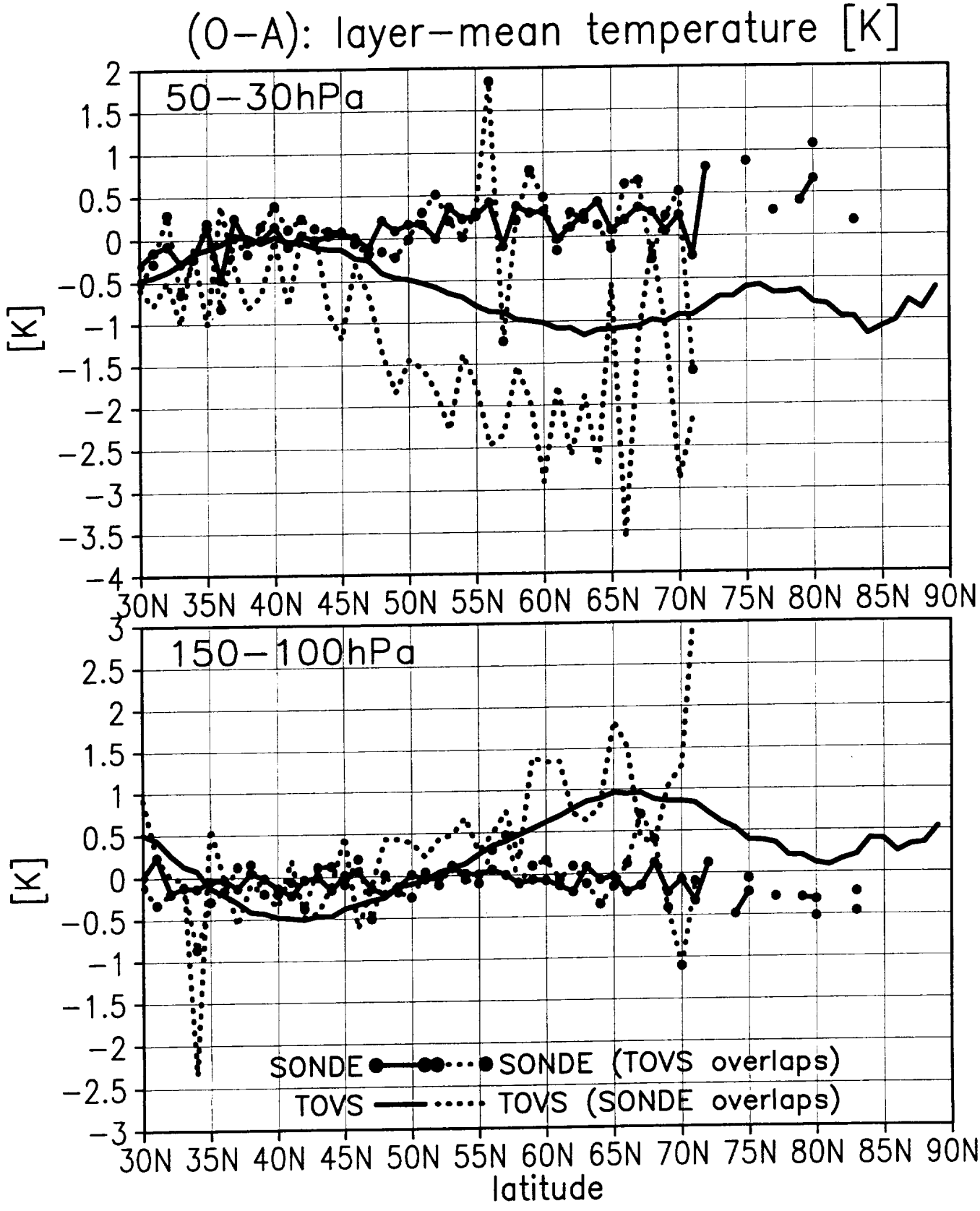
(O−A): layer−mean temperature [K]
50−30hPa
150−100hPa
[K]
2
1.5
1
0.5
0
−0.5
−1
−1.5
−2
−2.5
−3
−3.5
−4
3
2.5
30N 35N 40N 45N 50N 55N 60N 65N 70N 75N 80N 85N 90N
latitude
SONDE
SONDE (TOVS overlaps)
TOVS
TOVS (SONDE overlaps)

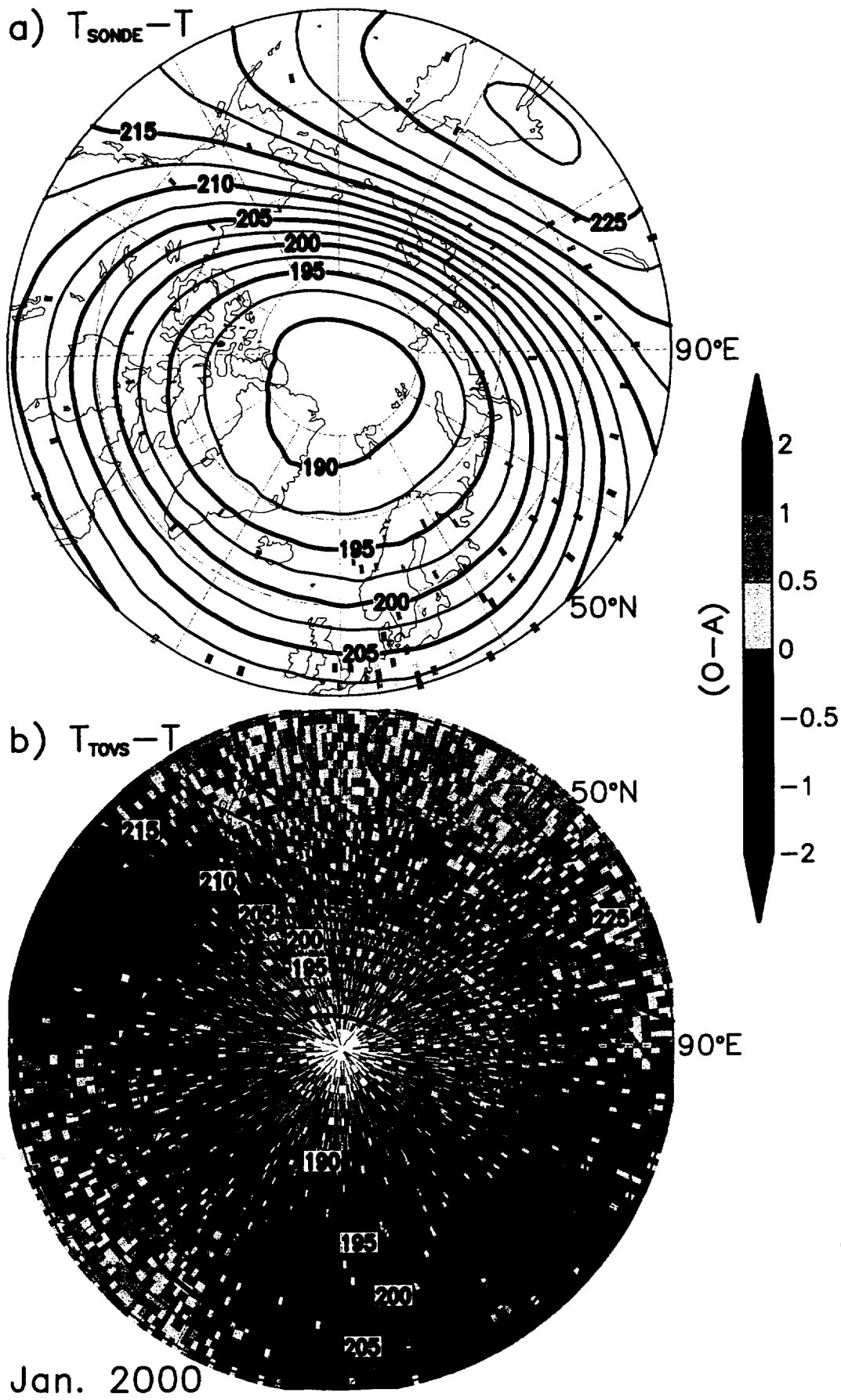

Plate1 (color)

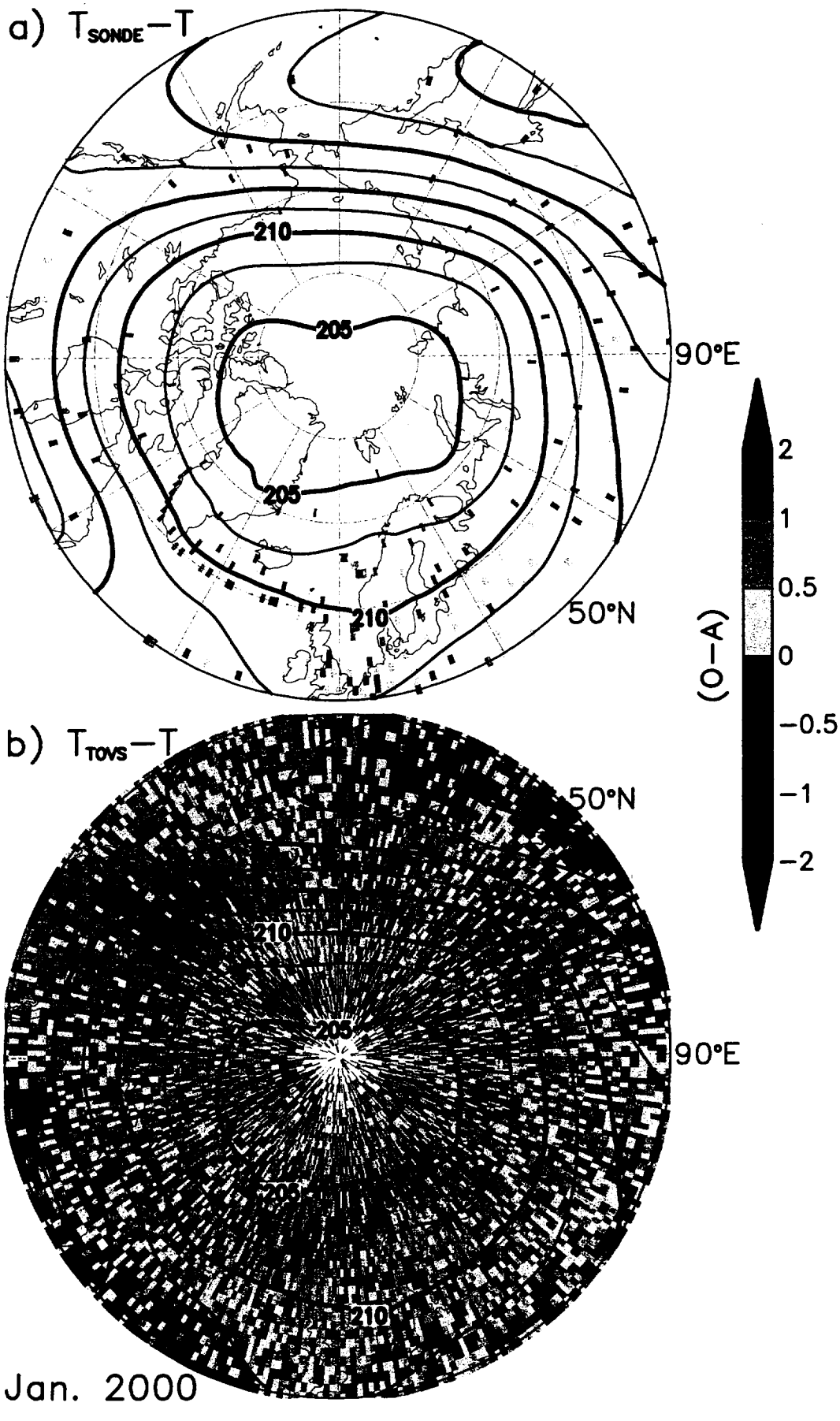

Plate 2 (color)

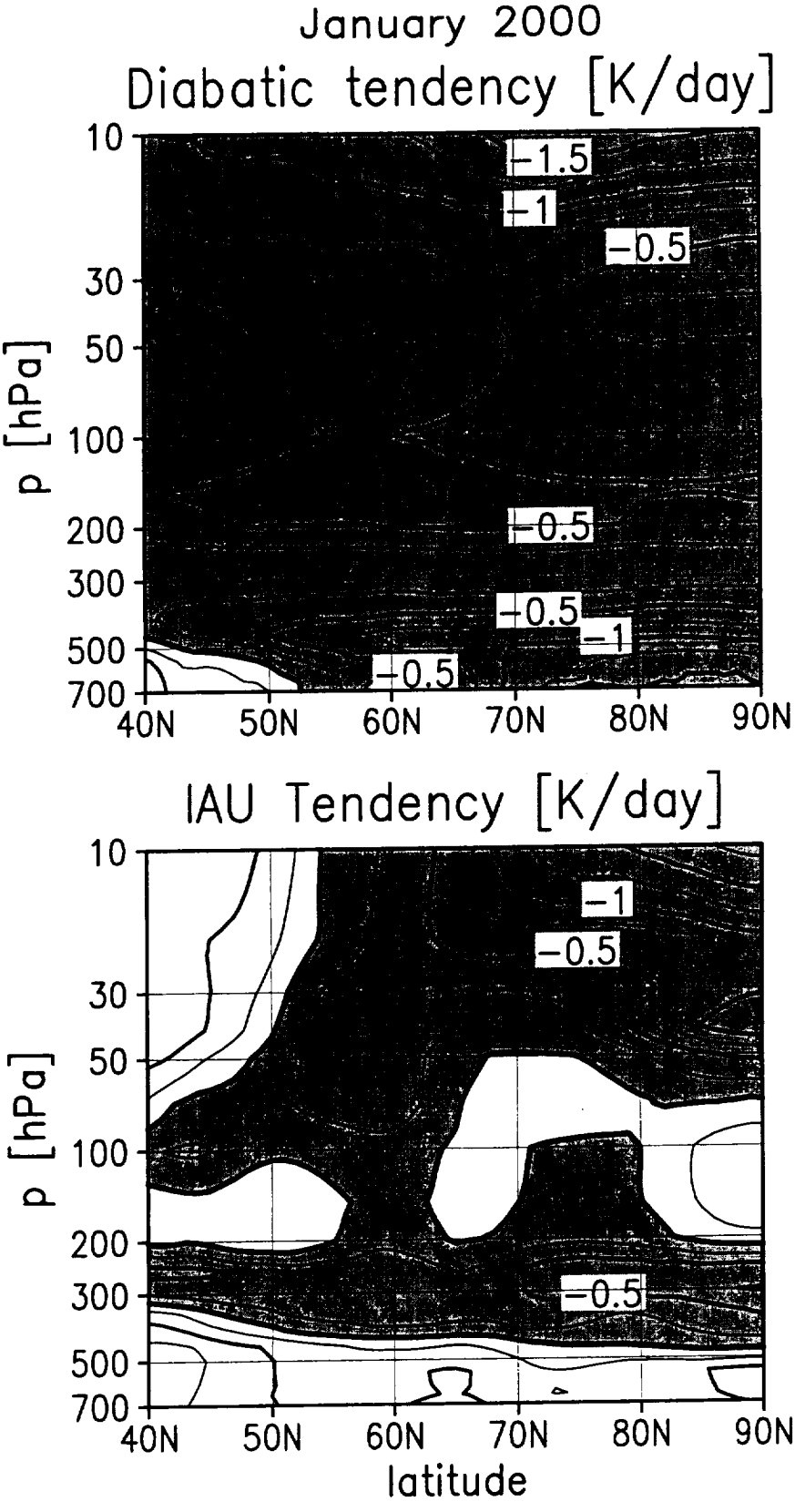
January 2000
Diabatic tendency [K/day]
10
30
50
100
200
300
500
700
p [hPa]
−1.5
−1
−0.5
−0.5
−0.5
−1
−0.5
40N
50N
60N
70N
80N
90N
IAU Tendency [K/day]
10
30
50
100
200
300
500
700
p [hPa]
−1
−0.5
−0.5
40N
50N
60N
70N
80N
90N
latitude

Fig 6

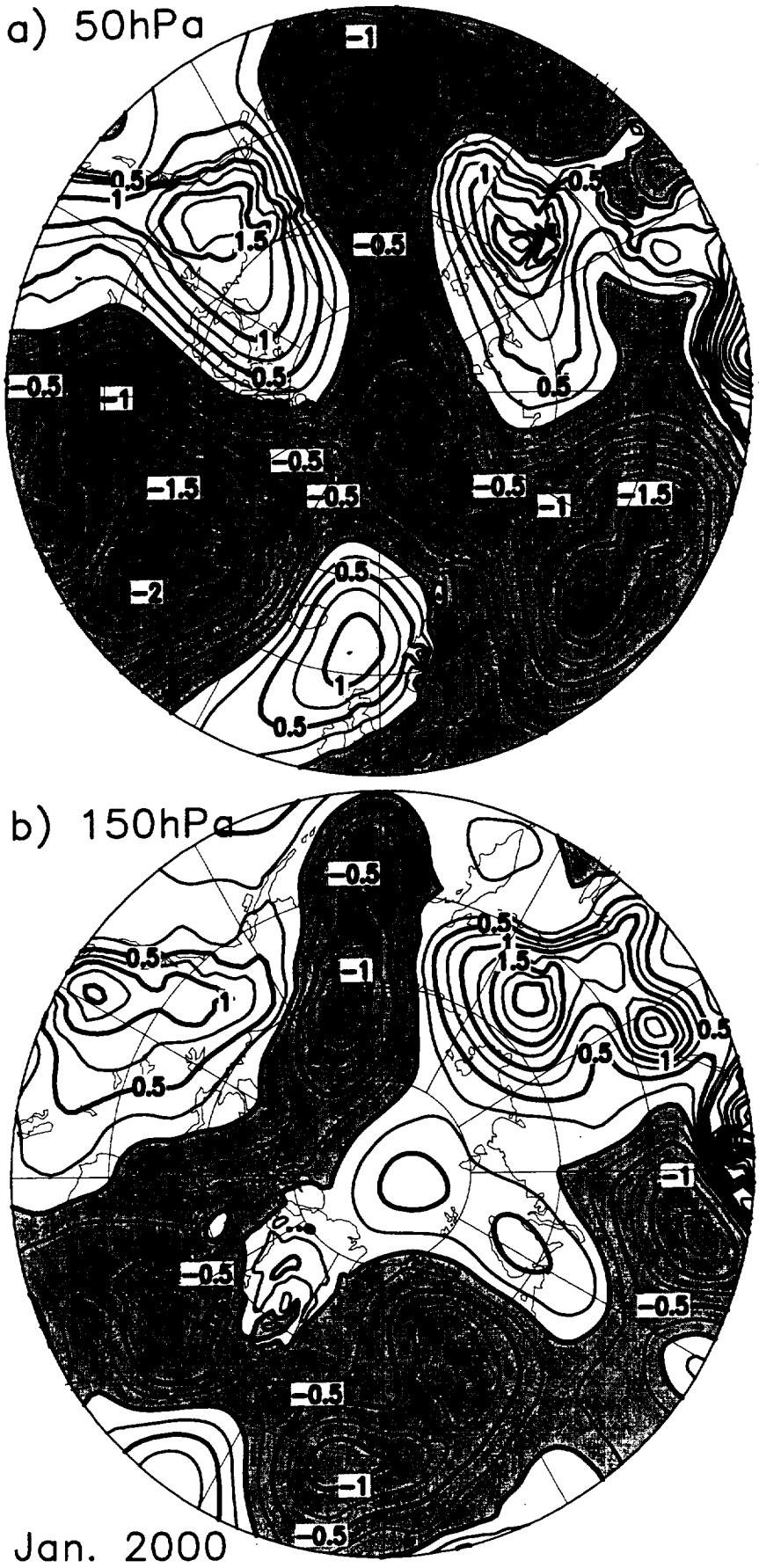

Fig 7

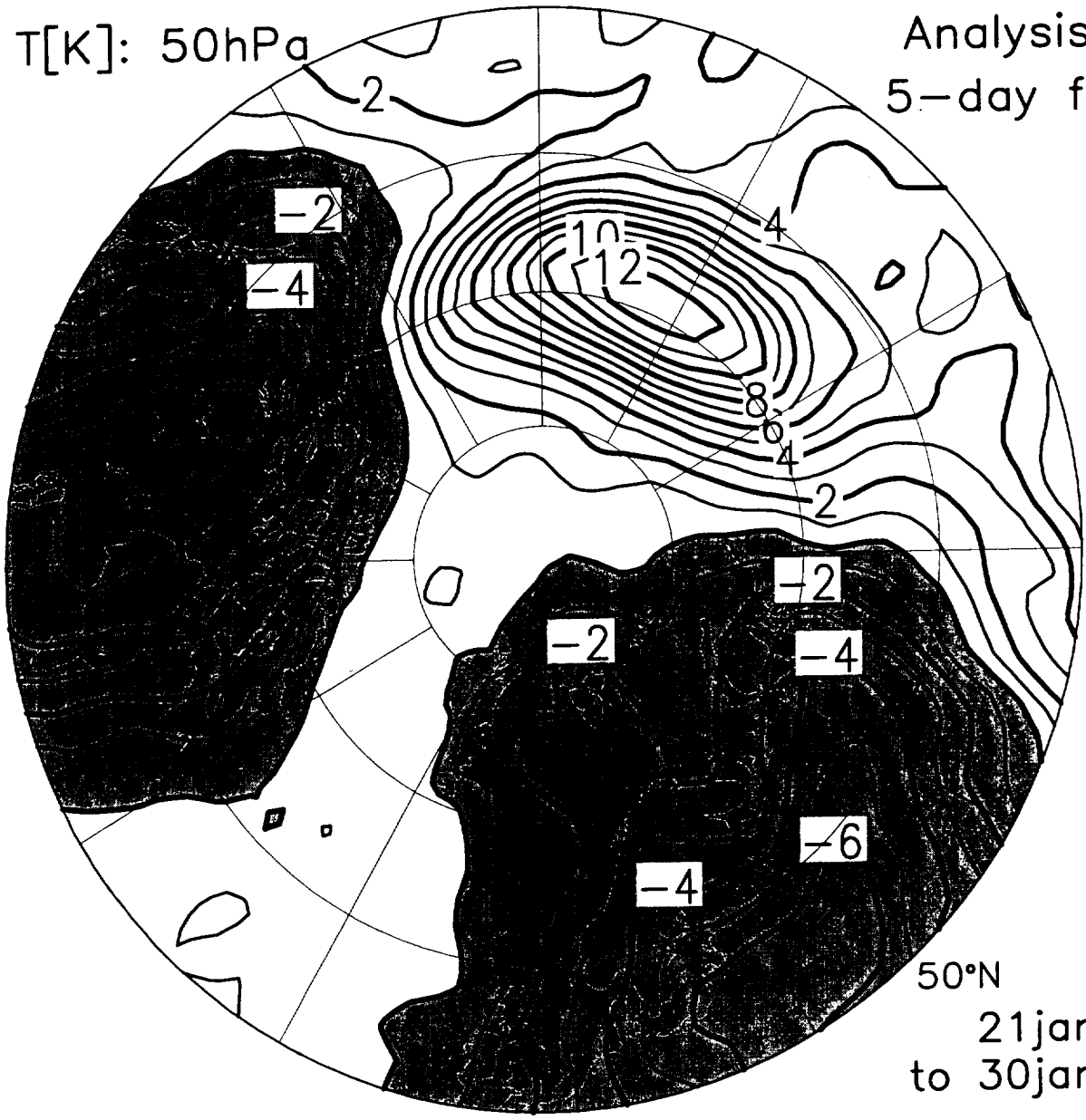
T[K]: 50hPa
Analysis minus
5–day forecast
2
–2
–4
10
12
4
8
6
4
2
–2
–2
–4
–6
–4
50°N
21jan2000
to 30jan2000

Fig 8

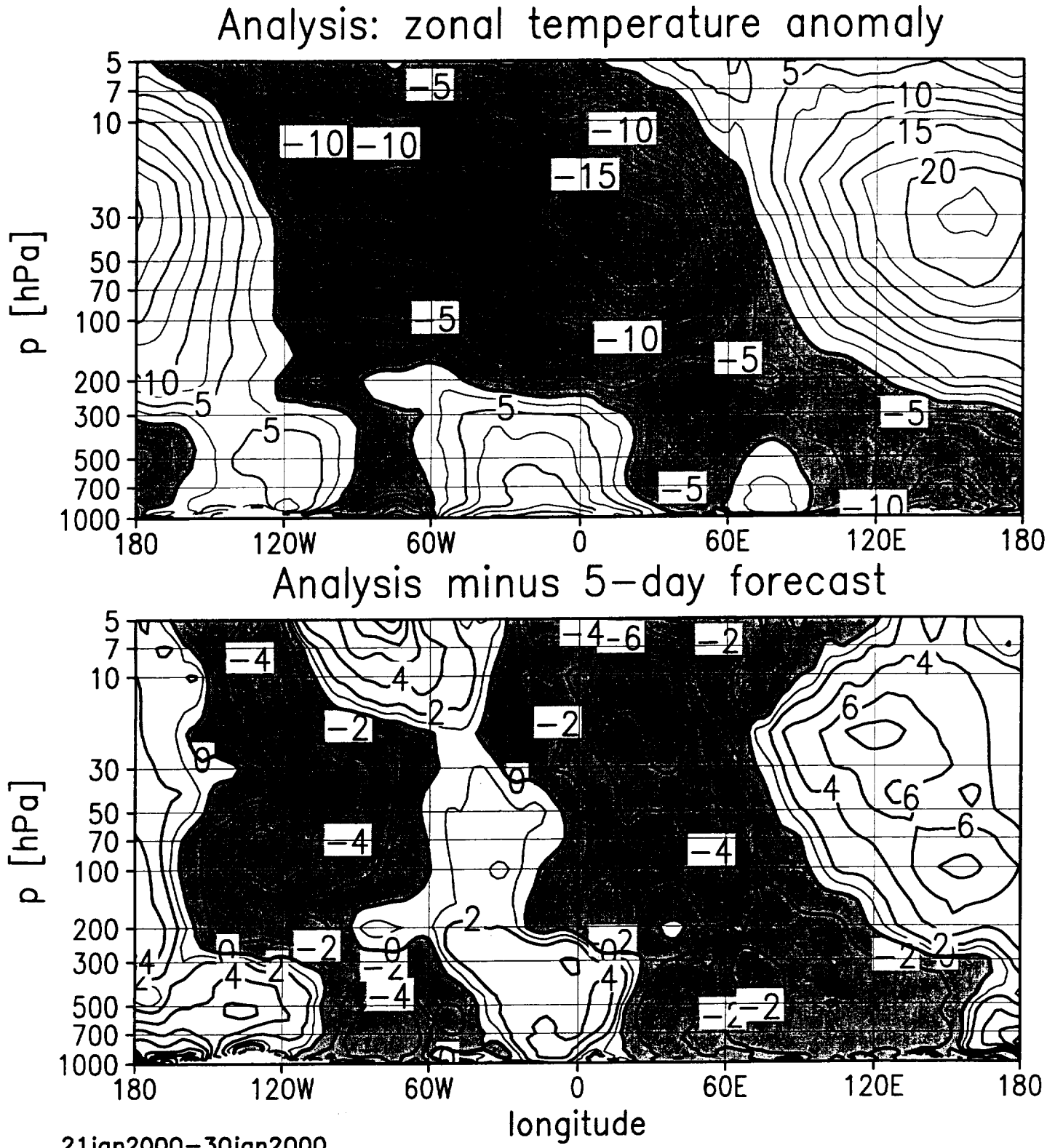
Analysis: zonal temperature anomaly
p [hPa]
5
7
10
30
50
70
100
200
300
500
700
1000
180
120W
60W
0
60E
120E
180
Analysis minus 5-day forecast
longitude
21jan2000–30jan2000

Fig 9

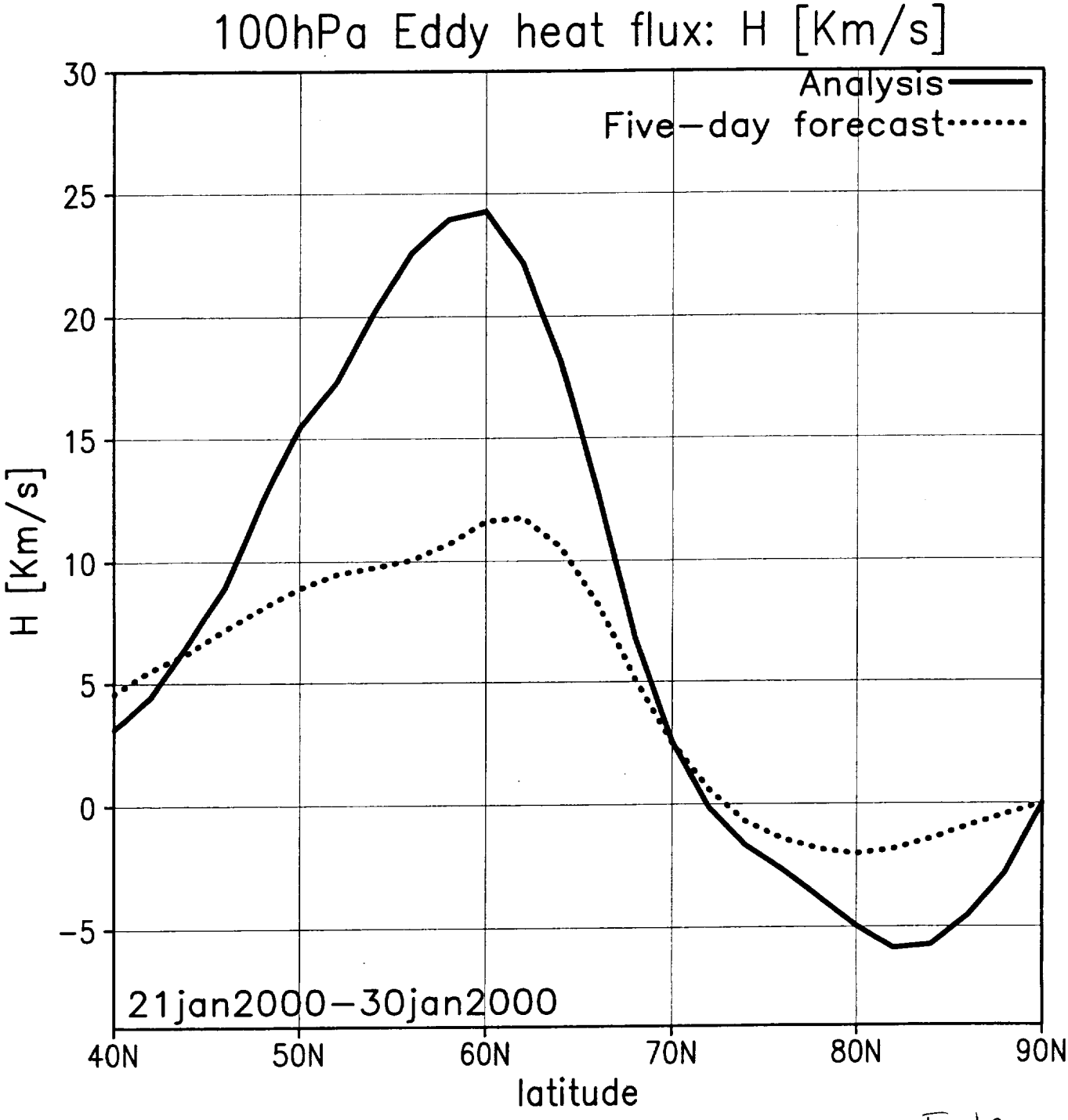
100hPa Eddy heat flux: H [Km/s]
Analysis
Five-day forecast
H [Km/s]
30
25
20
15
10
5
0
-5
21jan2000-30jan2000
40N
50N
60N
70N
80N
90N
latitude

Fig 10

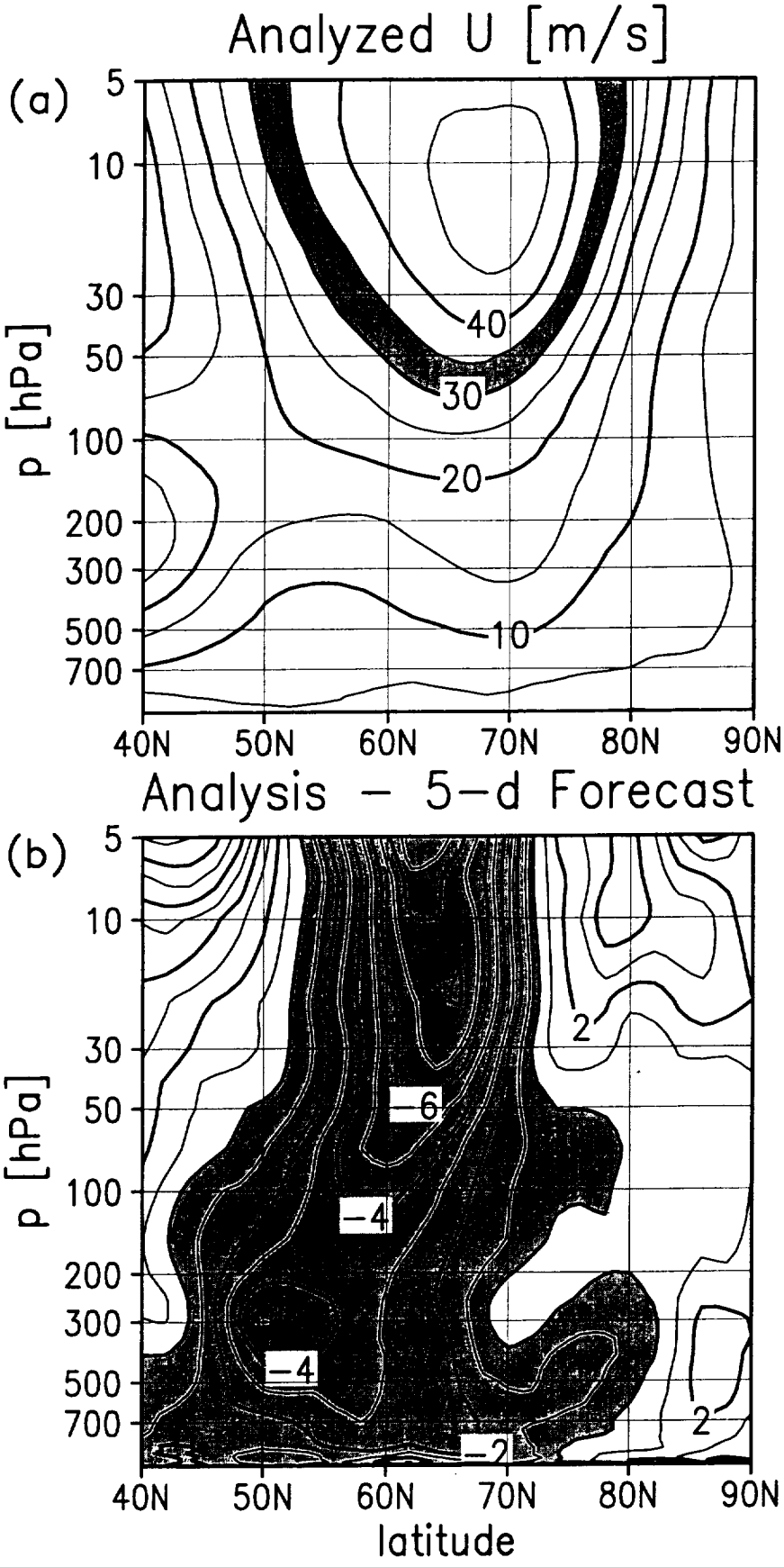

21jan2000−30jan2000

Fig 11

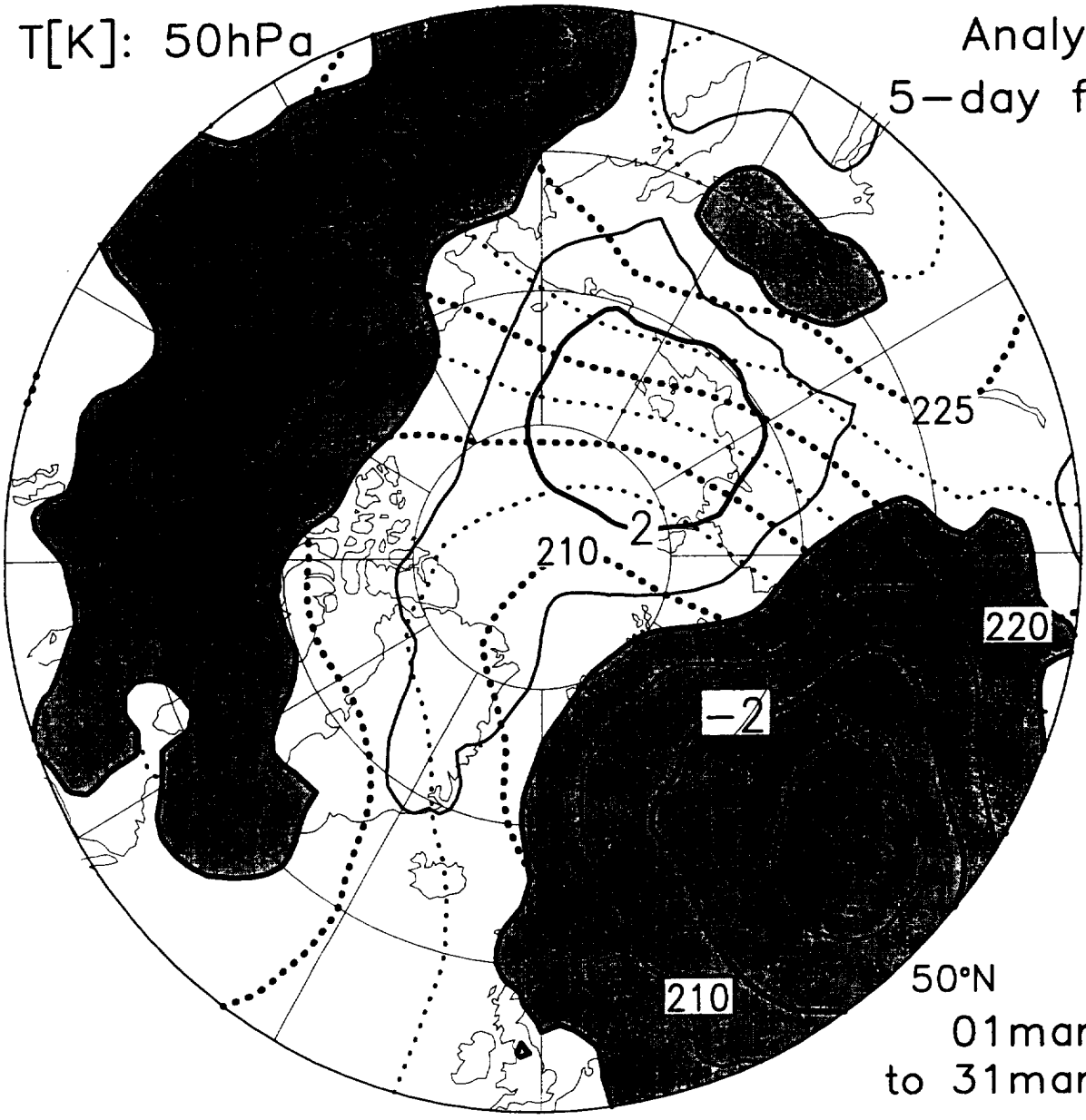
T[K]: 50hPa
Analysis and
5-day forecast
bias
225
2
210
220
-2
210
50°N
01mar2000
to 31mar2000

Fig 12

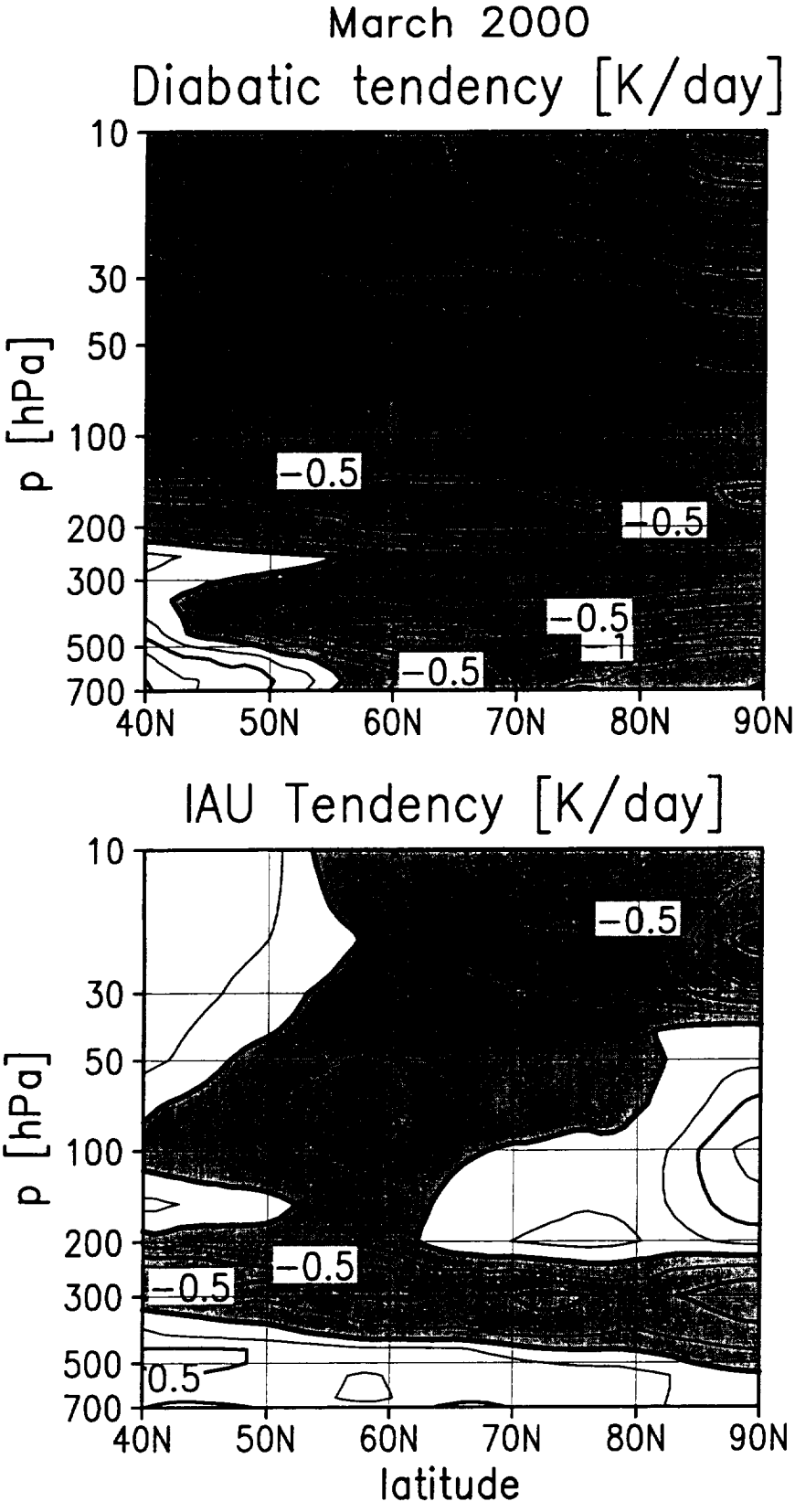
March 2000
Diabatic tendency [K/day]
10
30
50
100
200
300
500
700
p [hPa]
-0.5
-0.5
-0.5
-1
-0.5
40N
50N
60N
70N
80N
90N
IAU Tendency [K/day]
10
30
50
100
200
300
500
700
p [hPa]
-0.5
-0.5
-0.5
0.5
40N
50N
60N
70N
80N
90N
latitude

Fig 13

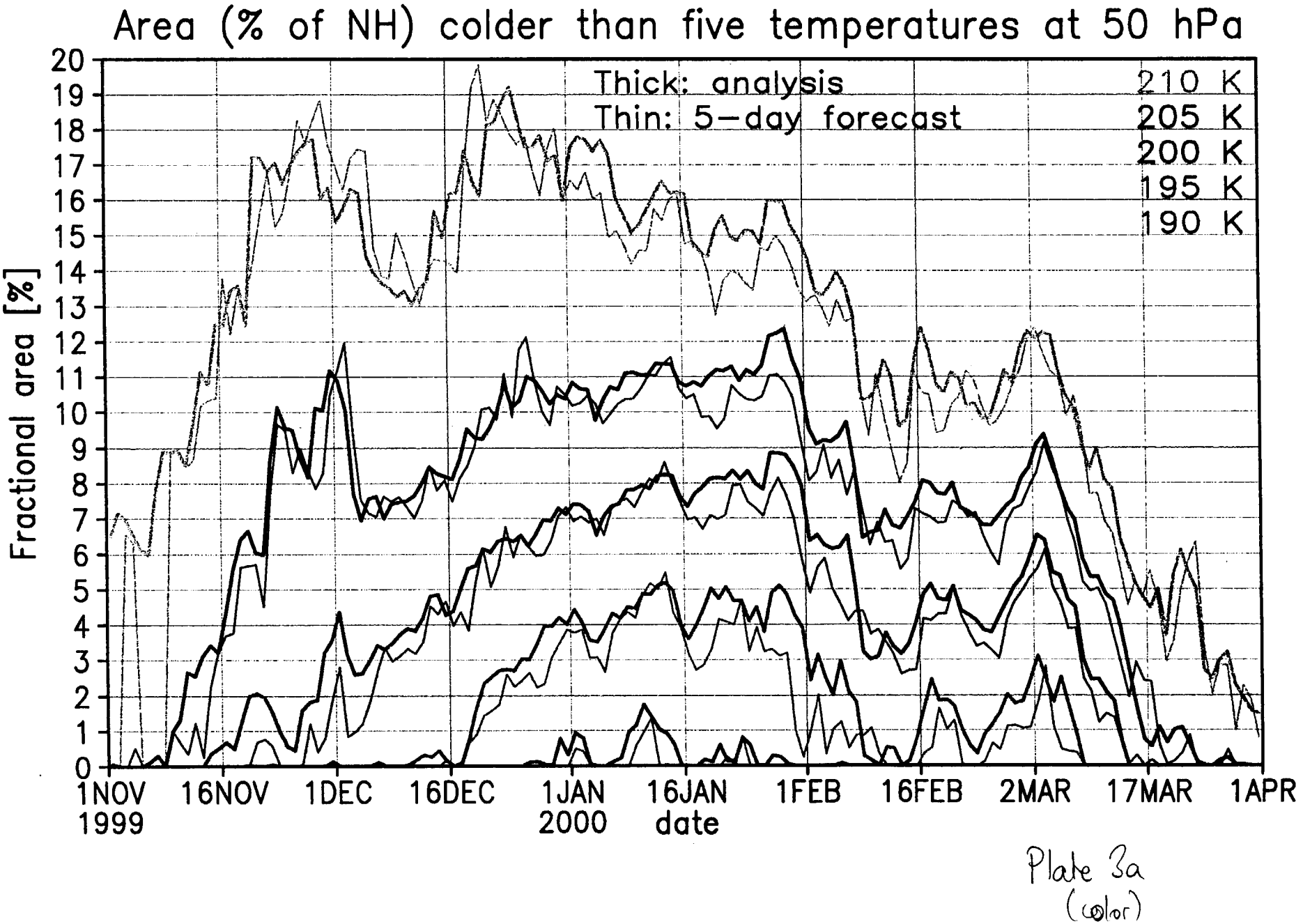

Plate 3a
(color)

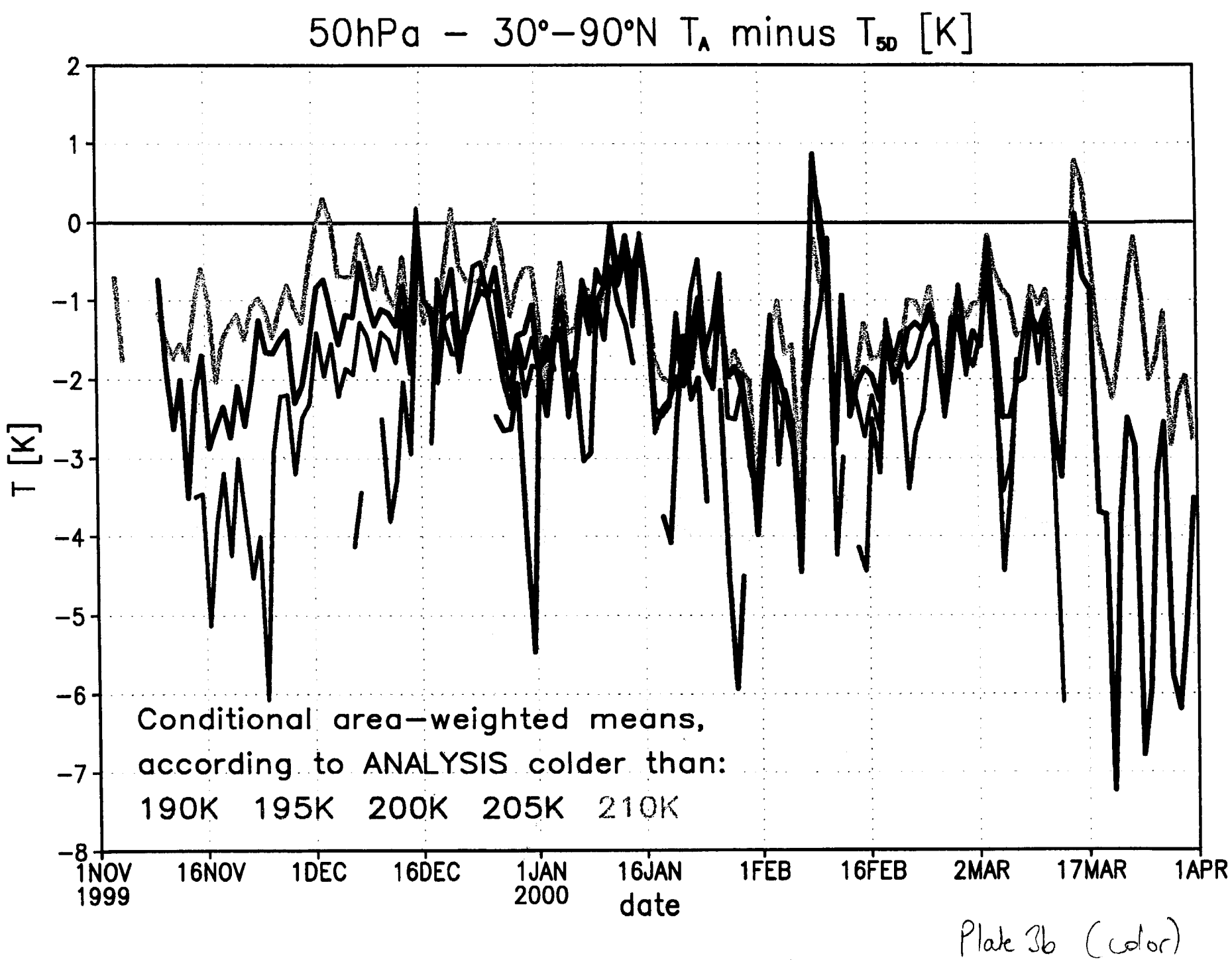

Plate 3b (color)